The Development of Electrochemical Systems for the Oxidation of Organic Contaminants for Water Treatment

by

Nyhenflore Hershelle Delva

A thesis

presented to the University of Waterloo

in fulfillment of the

thesis requirement for the degree of

Master of Science

in

Chemistry

Waterloo, Ontario, Canada, 2024

© Nyhenflore Hershelle Delva 2024

Author's Declaration

I hereby declare that I am the sole author of this thesis. This is a true copy of the thesis, including any required final revisions, as accepted by my examiners.

I understand that my thesis may be made electronically available to the public.

Abstract

1,4 dioxane, also known as dioxane, is a contaminant of emerging concern, with no natural methods of degradation and no established treatment methods. This study investigates the use of both direct and indirect electrochemical advanced oxidation processes to generate radicals for dioxane oxidation, and how adjusting electrochemical parameters may be used to tune dioxane oxidation towards target compounds, thus offering a pathway to combine wastewater treatment with the synthesis of valuable compounds. Ion chromatography and nuclear magnetic resonance were used to identify and quantify the liquid products. The electro-Fenton process was used to indirectly oxidize dioxane via the activation of H_2O_2 generated *in situ*. H_2O_2 was quantified using $TiOSO_4$ in an acidic solution. It was found that perfluorinated sulfonic acid binders can tailor carbon materials towards H_2O_2 production in acidic media, with as little as 5 wt% of PFSA binder dramatically improving both current density and H_2O_2 selectivity. Fe^{2+} concentration was shown to shift product selectivity of the Electro-Fenton process, with higher concentration resulting in greater selectivity towards C_1 products. Early analysis of anodic oxidation of dioxane on ZnO reveals that carbonate radicals- formed from the oxidation of the bicarbonate electrolyte- are also part of the oxidation pathway, resulting in a different range of products than previously documented in the literature.

Acknowledgements

I would like to thank Anna Klinkova for her excellent work as my supervisor. Her faith in my work and her dedication to seeing me succeed has motivated me more than I can say. I will forever be thankful for her patience and competence.

Secondly, I would like to thank my committee members: Holger Kleinke and Rodney Smith, for their time and consideration throughout my Master's.

I must also thank Xenia Medvedeva for being a constant source of support in the lab. Her generosity with both her brilliance and her companionship kept my experiments on track and my spirits high.

I cannot be writing acknowledgements without mentioning Jury Medvedev, who has been behind me every step of my graduate career, and whose considerable planning and good taste in movies have helped guide me through this chapter of my studies.

I'd also like to thank Yujie Liu for her boundless kindness and enthusiasm, which helped me to stay motivated and upbeat for many long nights in the lab.

Last but not least I'd like to thank my family and friends for their support, consideration, and patience.

Table of Contents

Author's Declaration ii

Abstract iii

Acknowledgements iv

List of Figures vii

List of Tables x

List of Abbreviations xi

Chapter 1 Introduction 1

1.1 Dioxane Production and Presence as a Waste-Water Contaminant 1

1.2 The Electro-Fenton Process 6

1.3 H_2O_2 Production via Oxygen Reduction Reaction in Acidic Environments 7

1.4 Direct Electrochemical Oxidation of 1,4 Dioxane 11

1.5 Scope of Thesis 14

Chapter 2 Methods and Materials 15

2.1 Catalyst Fabrication 15

2.1.1 Fabrication of PFSA:CB (5% w/w) Cathode 15

2.1.2 Electrodeposition of ZnO Anode 15

2.2 Catalyst Characterization 16

2.2.1 X-ray Diffraction Analysis (XRD) 16

2.2.2 Electrochemical Assessment 16

2.3 Product Identification and Quantification 17

2.3.1 Nuclear Magnetic Resonance Spectroscopy (NMR) 17

2.3.2 Ion Chromatography (IC) 17

2.3.3 UV-Vis Spectroscopy 17

2.3.4 Gas Chromatography (GC) 18

Chapter 3 Experimental Results 19

3.1 Dioxane Oxidation Through Electro-Fenton Reaction 19

3.1.1 H_2O_2 Production on 5% Nafion:CB Catalyst in Acidic Media 19

3.1.2 Products of Dioxane Oxidation as a Factor of Fe^{2+} Concentration 26

3.2 Dioxane Oxidation on ZnO in Alkaline Media 29

3.2.1 The activity of ZnO Catalyst Towards $2e^-$ WOR 29

3.2.2 Product Selectivity as A Factor of Potential 31

Chapter 4 Conclusions and Outlook 33

Letters of Copyright Permission 35

References 39

Appendix A 44

List of Figures

Figure 1-1- The current methods of AOP-centered treatment options. Reprinted with permission from reference 2. 2

Figure 1-2- Scheme of $2e^-$ and $4e^-$ pathways seen in electrochemical ORR. Reprinted with permission from Reference 21 under the Creative Commons Attribution 4.0 International license. 8

Figure 1-3- (a) H_2O_2 FE% of carbon black in 0.1M H_2SO_4 with the addition of CTAB. (c) Schematic illustration of $2e^-$ ORR with/without Na^+. Reprinted with permission from Reference 32 under the Creative Commons Attribution 4.0 International license. (b) Schematic illustration of the electrical double layer on the carbon surface without and with CTAB from Reference 32 under the Creative Commons Attribution 4.0 International license. (c) Schematic illustration of $2e^-$ ORR with/without Na^+. Reprinted with permission from Reference 34 (d) H_2O_2 FE% of carbon black in 0.1M H_2SO_4 with/without Na^+ in 0.1M H_2SO_4. Reprinted with permission from Reference 34. (e) Illustration of the hydrophobic ($-CF_3$) and hydrophilic ($-SO_3^-$) motifs seen in Nafion on copper catalyst supported on Gas diffusion electrode. Reprinted with permission from Reference 35. 10

Figure 1-4- (a) Schematic illustration of direct and indirect electrochemical anodic-oxidation pathways for organic compounds. Adapted with permission from Reference 9 (b) Schematic of flow cell producing H_2O_2 on both cathode and anode through ORR and WOR, respectively. Reproduced with permission from Reference 20 (c) Selectivity diagram for WOR to H_2O_2 on various metal oxides. Reproduced with permission from Reference 41 (d) H_2O_2 FE% for various metal oxides at 3.0 V vs RHE. Reproduced with permission Reference 43. 13

Figure 3-1 FE% of H_2O_2 (a) and $j_{H_2O_2}$ (b) as a function of potential in 0.5M Na_2SO4 at pH 3 using 5% PFSA:CB and a carbon black-based electrode with no PFSA binder. (c) Schematic illustration of increased H_2O_2 selectivity through PFSA limiting proton availability. The negatively charged

sulphate end group motifs direct both proton and cations on the electrode surface, limiting adsorbed protons available for ORR and pushing reaction conditions towards $2e^-$ ORR. 20
Figure 3-2- Cyclic Voltammetry of CB catalyst with and without PFSA binder in 0.5M Na_2SO_4 at pH 3 using H_2SO_4 21
Figure 3-3- (a) Heat map displaying H_2O_2 FE% as a dependent of Na_2SO_4 concentration and potential in solutions of pH 3 using H_2SO_4. Current densities (b) and j_{H2O2} (c) as a function of potential in varying concentrations of Na_2SO_4 at pH 3 using 5% PFSA:CB. 23
Figure 3-4- (a) Heat map displaying H_2O_2 FE% as a function of pH and potential in a solution of 0.5M Na_2SO_4. Current densities (b) and j_{H2O2} (c) as a function of potential in 0.5M Na_2SO_4 at varying pH. 24
Figure 3-5- (a) CA of ORR at -0.3V in 0.5 M Na_2SO_4 electrolyte with pH 3. Symbols are used to denote H_2O_2 FE% for both catalysts: with and without PFSA binder. (b) H_2O_2 production rate for both catalysts during the eight-hour electrolysis. (c) Comparison of 5% PFSA:CB to other catalysts in literature. The full chart can be found in Supporting information. (Table 4) 25
Figure 3-6: Reaction pathway for direct oxidation of dioxane, as proposed by Jasmann et al. Reproduced with permission from Reference 10. 27
Figure 3-7- (a) Dioxane conversion as a function of Fe^{2+} concentration after passing 500 C through the carbon electrode. (b) FE% of products, including H_2O_2, formed in the cathodic compartment after passing 250C and 500C. (c) Dioxane conversion (%) and product selectivity (%) of EF-facilitated dioxane oxidation after 500C has passed. ..... **Error! Bookmark not defined.**
Figure 3-8- XRD analysis of (a) electrodeposited ZnO onto carbon paper substrate with (b) ZnO and (c) Aluminum as reference. Cyclic voltammetry was performed for (d) ZnO in 2M $KHCO_3$ - with and without dioxane- with (e) CB as a control. 30

Figure 3-9- (a) Dioxane conversion (%) and product selectivity (%) of dioxane oxidation on ZnO in 2 M $KHCO_3$ after 500C has passed. (b) IC chromatograph of long-term dioxane oxidation at an applied potential of 2.2V. (c) Cyclic voltammetry of ZnO with 0.1 M dioxane in 2M $KHCO_3$ (red) and 2M KNO_3 (blue). 31

Figure 5-4- Calibration curve of H_2O_2/Ti complex. The wavelength of interest was 409nm. The R^2 value was 0.9915. 44

Figure 5-5- NMR Standards of Common Dioxane Oxidation Products as Determined by Jasmeen et al 50

Figure 5-6- ^{13}C NMR (top) and ^{1}H NMR (bottom) of EF reaction at 3mM Fe^{2+} after 500C has passed. Peaks of interest are identified. 51

Figure 5-7- IC results containing ionic products formed during long-term EF reaction at 5mM Fe^{2+} .52

List of Tables

Table 1- Parameters of Electrochemical AOPs Used to Degrade 1,4-Dioxane 3

Table 2- Calculation of the Total Costs of Electrochemical Oxidation and Photo-Fenton processes for the Treatment of 1,4-Dioxane Contaminated Wastewater until 40% COD Removal at a Rate of 43 800 $m^3 \cdot y^{-1}$ * 5

Table 3- Recently Developed Treatment Systems Utilizing AOPs for 1,4-Dioxane Degradation 44

Table 4- List of Electrocatalysts Recently Developed for 2e- ORR in Acidic Media with the Electrolyte Used in the System, Onset Potential, FE% at Greatest Current Density, and the Percentage of Nafion (w/w%) Used in the Catalyst Ink 47

List of Abbreviations

AOP	Advanced Oxidation Process
BDD	Boron Doped Diamond
CB	Carbon Black
COD	Chemical Oxygen Demand
CTAB	Cetyltrimethylammonium bromide
EF	Electro-Fenton
EPA	U.S. Environmental Protection Agency
FE%	Faradaic Efficiency %
GC	Gas Chromatography
HER	Hydrogen Evolution Reaction
IC	Ion Chromatography
NMR	Nuclear Magnetic Resonance
ORR	Oxygen Reduction Reaction
PFSA	Perfluorinated Sulfonic Acid
PTFE	Poly(tetrafluoroethylene)
ROS	Reactive Oxidizing Species
WOR	Water Oxidation Reaction
XRD	X-ray Diffraction

Chapter 1

Introduction

1.1 Dioxane Production and Presence as a Waste-Water Contaminant

1,4-Dioxane, also known as dioxane, is a heterocyclic ether that was historically used as a solvent stabilizer for chlorinated solvents such as 1,1,1-trichloroethane.[1] Currently, it is used in the manufacturing processes of various industries such as pharmaceuticals, personal care products, and cosmetics.[2] Though its usage has significantly declined following the phase-out of 1,1,1-trichloroethane under the Montreal Protocol, 1,4-dioxane is still produced at volumes exceeding 1 million pounds annually.[1] Due to its low volatility and high solubility in water, 1-4-dioxane is commonly found in surface and groundwater. In the early 2000s, the EPA classified 1,4-dioxane as a contaminant of emerging concern, labelling it a possible carcinogen and a known irritant with no established treatment methods.

Due to its stable ring structure, current treatment technologies focus on using advanced oxidation processes (AOP) to degrade dioxane.[2,3] AOPs are degradation processes that rely on the generation of highly reactive oxidizing species (ROS), such as hydroxyl radicals (·OH), to oxidize persistent contaminants in wastewater.[3] Examples of these processes are illustrated in **Figure 1-1** below.

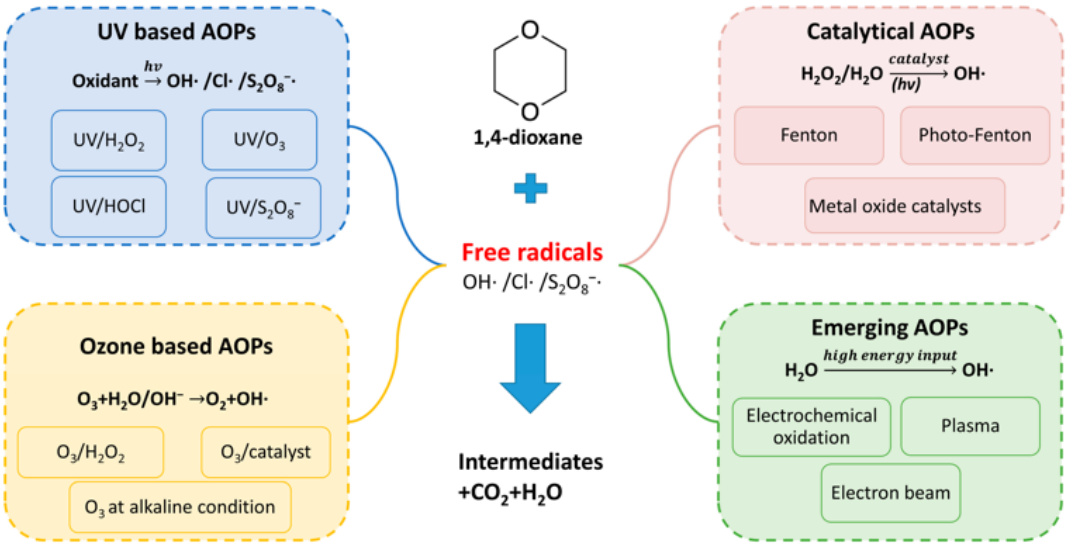


Figure 1-1- The current methods of AOP-centered treatment options. Reprinted with permission from Reference 2.

Most work in dioxane oxidation with conventional AOPs has focused on using UV/H_2O_2 AOP processes, where UV light provides the energy necessary to either directly activate H_2O_2, or facilitate a Fenton reaction, where metals favouring one electron transfers can react with hydrogen peroxide in solution to produce hydroxyl radicals.[4,4–7] UV/H_2O_2 systems are commonly used in wastewater treatment and are well-established for dioxane treatment.[1,6,8] A full-scale operation implemented at a site in Michigan reports a 99.95% 1,4-dioxane removal, treating 5000 gallons of contaminated water daily.[1] However, this method often requires a large excess of the initial H_2O_2 (~19x the volume of the 1,4-dioxane), increasing operational costs.[8] Electrochemical oxidation uses electricity to generate highly oxidizing oxygen species (ROS) *in situ*, typically through an inert anode such as boron-doped diamond (BDD).[1,9] This eliminates the need to purchase and store large amounts of strong oxidizing agents such as H_2O_2. Electrochemical systems are already being used to degrade 1,4-dioxane, as seen in **Table 1**. Additionally, by changing electrochemical parameters such as

electrolyte, dioxane concentration, and potential, it's possible to shift product selectivity and performance of the electrochemical system.[10,11] This offers the opportunity to shift dioxane oxidation from being simply wastewater treatment to potentially a means of generating valuable organic compounds.

Table 1- Parameters of Electrochemical AOPs Used to Degrade 1,4-Dioxane

Electrodes	Electrochemical conditions	Dioxane Oxidation	Reference
Ti/TiONC/Sb-SnO_2	0.1 M Na_2SO_4 with 0.11 mM 1,4- dioxane	~100% Dioxane Degradation by 2 hr **No Product Analysis**	12
BDD	0.1M Na_2SO_4 at 6V with 0.1 M dioxane	~100% Dioxane Removal by 2 hr **No Product Analysis**	13
1% Graphene Oxide Nanoparticles@ Ti_4O_7	0.02 M Na_2SO_4 at 6V with 0.01 M dioxane	63.2% Dioxane Removal in 0.012h **No Product Analysis**	14
TiO_2	0.03M Na_2SO_4 at 8V with 0.34 mM Dioxane	85.2% Dioxane Removal by 0.107 hr **Qualitative Product Analysis**	10

Table 2, adapted from reference 15, compares the total costs of operating 1-4-dioxane treatment plants using photo-Fenton ($UV/Fe^0/H_2O_2$) to that by electrochemical oxidation. The total cost of AOP treatment is depends on its capacity and operating process. In the study by Barndõk et al., the plant size and oxidant requirements were determined to be at which point the plant would be able to degrade dioxane-containing wastewater (248 ± 12 mg·L^{-1} of dioxane) to 40% chemical oxygen demand (COD) at a rate of 43 800 $m^3 \cdot y^{-1}$. The cost and size of the plants to meet this demand were calculated using experimentally determined amounts of oxidants and current literature on the target AOPs.[15]

Using the above criteria, it is shown that the annual operational costs of the photo-Fenton reaction are higher than that of electrochemical oxidation (€151,936 vs €128,489) due to the costs associated with purchasing and handling chemicals. However, the capital costs of the electrochemical oxidation process are much higher due to the expensive BDD electrodes. Cheaper or more readily available materials for the electrocatalysts would see electrochemical oxidation become more competitive as a potential wastewater treatment process for dioxane. Merging conventional AOPs, which indirectly generate ROS, with electrochemical processes may make it possible to combine lower capital costs seen in conventional AOPs with the flexibility afforded by electrochemical AOP. One such electrochemical AOP is the electro-Fenton (EF) process.

Table 2- Calculation of the Total Costs of Electrochemical Oxidation and Photo-Fenton processes for the Treatment of 1,4-Dioxane Contaminated Wastewater until 40% COD Removal at a Rate of 43 800 $m^3 \cdot y^{-1}$ *

	Electrochemical Oxidation (BDD)	***Photo-Fenton ($UV/Fe^0/H_2O_2$)***
	Capital Investment	
Total Capital Investment	1,013,566	273,590
Annual Capital Investment	97,649	26,358
	Operation and Maintenance Costs	
Energy	59,218	58,632
Chemicals	5,830	29,912
Repairs and Maintenance	26,441	26,392
Annual Operational Costs (y^{-1}) **	128,489	151,936
Total Annual Cost (y^{-1})	**226,138**	**178,294**

*All costs are in €

**Includes costs of labor (€25,000) and analytical monitoring (€12,000)

1.2 The Electro-Fenton Process

The conventional Fenton process uses Fe^{2+} and H_2O_2 to generate hydroxyl radicals to oxidize organic compounds non-selectively and has exhibited use in dioxane degradation.[7,16,17] However, like other conventional AOPs, there are high costs and risks related to storing, transportation, and handling of H_2O_2. Additionally, the process generates iron sludge as a byproduct during treatment. In contrast, the EF process utilizes electricity to generate H_2O_2 *in situ* on the cathode through the oxygen reduction reaction (ORR) (**Eq 1**). Aqueous Fe^{2+} ions then react with H_2O_2 to produce hydroxyl radicals (**Eq 2**). The Fe^{2+} catalyst is regenerated via the reduction of Fe^{3+} at the cathode, as seen in **Eq 3**.

$$O_2 + 2H^+ + 2e^- \rightarrow H_2O_2 \quad (1)$$

$$Fe^{2+} + H_2O_2 \rightarrow Fe^{3+} + OH^- + HO^{\cdot} \quad (2)$$

$$Fe^{3+} + e^- \rightarrow Fe^{2+} \quad (3)$$

This process has some advantages over the conventional Fenton reaction by: (1) removing the costs associated with producing H_2O_2 *ex-situ*, (2) removing the costs associated with the removal of iron sludge, and (3) the original Fe^{2+} catalyst can be regenerated quicker on the cathode than through side reactions.[18] It also has advantages over current electrochemical dioxane oxidation systems by using the Fe^{2+}/Fe^{3+} catalyst cycle to generate hydroxyl radicals, eliminating the two main disadvantages: expensive catalysts and large voltages.

Like other electrochemical oxidation reactions, EF processes allow one to control product selectivity and efficiency by adjusting the reaction parameters such as cell potential, current, or electrolyte. One such example can be seen in a work by Sheng et al, using EF to oxidize glycerol to form target C_3^+ products while simultaneously also oxidizing glycerol in the anodic chamber.[19] The

authors could shift the reaction's product selectivity by shifting parameters such as iron concentration and potential. The EF process offers a means to explore potential value in the products of dioxane oxidation and the means to tune product selectivity, an advantage that has yet to be explored in systems for dioxane oxidation as seen in **Table 3.**

1.3 H_2O_2 Production via Oxygen Reduction Reaction in Acidic Environments

The main difference between the Electro-Fenton process and the conventional Fenton process is the generation of H_2O_2 *in situ*.[16] While the electrosynthesis of H_2O_2 was less efficient than chemical synthesis initially, further work on understanding the kinetics of the $2e^-$ ORR and the $2e^-$ water oxidation reaction (WOR) to H_2O_2 has led to electrocatalysts with high current densities and/or H_2O_2 selectivity.[20] Generally, ORR proceeds via two pathways: dissociative or associative pathways as seen in **Figure 1-2**.[21] In the dissociative pathway, the O-O bond is broken as the oxygen atoms of O_2 are adsorbed onto two different active sites. This pathway results in $4e^-$ ORR to form H_2O. In the associative pathways, the O-O bond is preserved as O_2 is adsorbed onto the surface of the catalyst. Once adsorbed, O_2 reacts with protons in solution to form an $^*OOH$ intermediate.[22] From there, *OOH may combine with another proton to form H_2O_2, or it may dissociate to form *O and *OH and continue to form H_2O via the $4e^-$ ORR pathway.

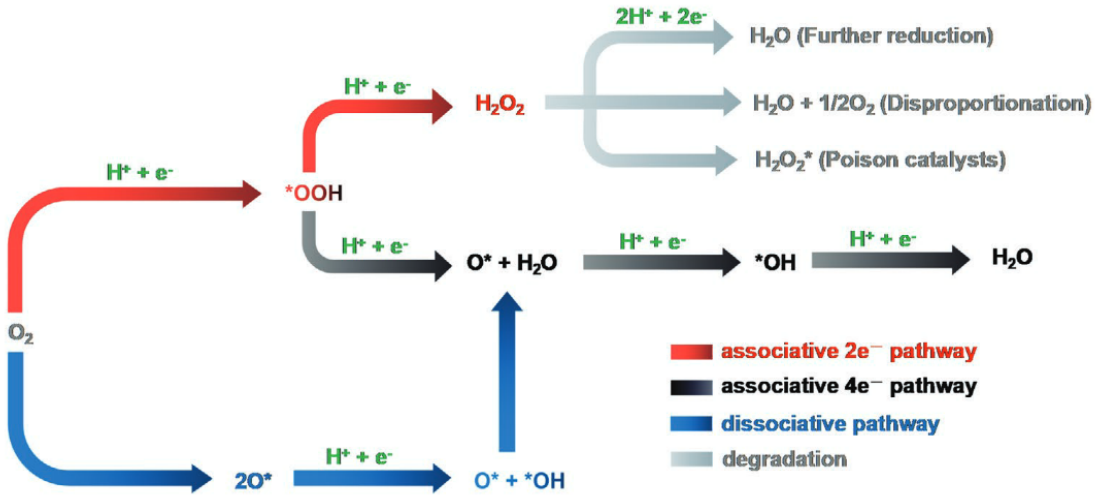


Figure 1-2- Scheme of $2e^-$ and $4e^-$ pathways seen in electrochemical ORR. Reprinted with permission from Reference 21 under the Creative Commons Attribution 4.0 International license.

Typically, catalyst design efforts have focused on developing materials with strong adsorption of O_2 and weak adsorption of the $^*OOH$ intermediate- preferring ORR over other competing reactions such as hydrogen evolution reaction (HER) and decreasing the time $^*OOH$ spends on the catalyst surface, thus favouring the $2e^-$ ORR pathway.[21] Historically, noble metals and their alloys have been the preferred materials for $2e^-$ ORR, due to their small overpotentials and high selectivity (>90%), as seen in Error! Reference source not found..[21,23–25] However, due to their scarcity and high cost, work has been done on developing catalysts using more accessible materials, such as carbon-based materials.[26–30] Carbonaceous materials have shown promise as an alternative catalyst material due to their tunability, abundance, and low costs compared to noble metals.[31] Carbon-based materials also have high selectivity towards $2e^-$ ORR and low overpotential in alkaline media, making them popular for electrochemical H_2O_2 generation.[20] Most efforts in electrochemical

H_2O_2 generation on carbon-based materials are done in alkaline media due to the small overpotential and the high selectivity towards $2e^-$ ORR due to the limited availability of protons.[20,21,26–28,31] However, H_2O_2 is less stable in alkaline media due to ^-OH catalyzing the decomposition of H_2O_2 to water and oxygen, and the EF process requires a pH between ~2.8-3 to maximize the solubility of the Fe^{2+} catalyst. [16,20]

One strategy for achieving high selectivity towards $2e^-$ in acidic media is to replace the protons on the catalyst surface with other positive charges, creating a microenvironment with a high pH on the catalyst surface.[32–34] One such example was shown in a work by Adler et al., where the H_2O_2 faradaic efficiency % (FE%) of ORR on a carbon black catalyst increased from 13% to 95% at -200 mA cm^{-2} upon the addition of 10mM cetyltrimethylammonium bromide (CTAB) to the 0.1M H_2SO_4 electrolyte (seen in **Figure 1-3a**).[32] As seen in the illustrated schematic (**Figure 1-3b**), the authors suggested that CTAB forms micelles that are drawn to the catalyst surface due to the Coulombic attraction between the catalyst's negative charge and the positive charge of the molecules. This results in a hydrophobic microenvironment that deters protons from the surface, resulting in a higher selectivity towards $2e^-$ ORR over $4e^-$ ORR or HER. Another work by Zhang et al. demonstrated a similar Coulombic effect using alkali metal cations.[34] In a flow cell filled with 0.1M H_2SO_4 as an electrolyte, the carbon black catalyst had an H_2O_2 FE% of 35% at 200 mA cm^{-2}. Upon the addition of Na^+ cations (5mM Na_2SO_4), the H_2O_2 FE% increased to ~83% at 200 mA cm^{-2}. It was shown that the Na^+ cations compete with protons on the catalyst surface, reducing proton availability on the surface and increasing selectivity towards $2e^-$ ORR.

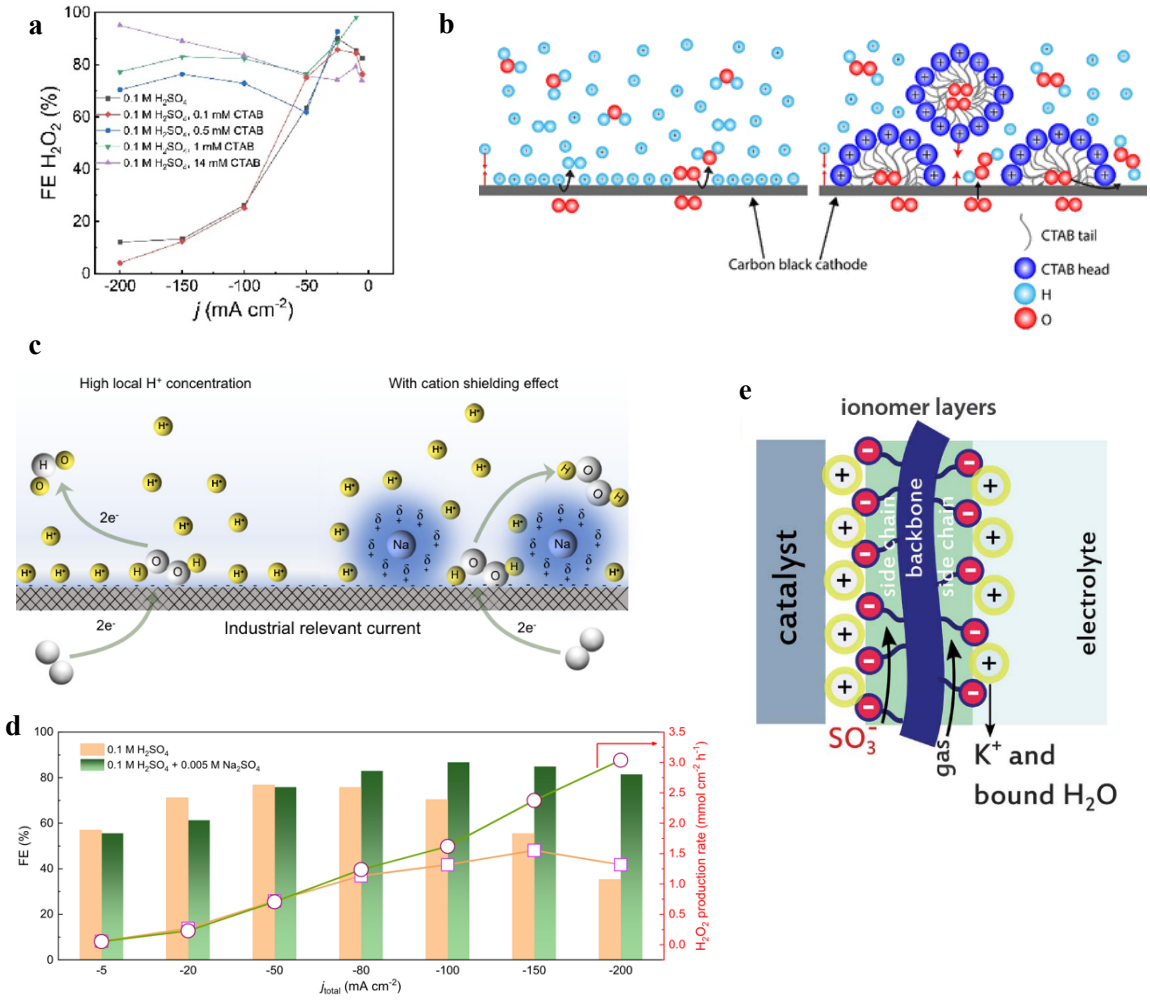


Figure 1-3- (a) H_2O_2 FE% of carbon black in 0.1M H_2SO_4 with the addition of CTAB. (c) Schematic illustration of 2e$^-$ ORR with/without Na^+. Reprinted with permission from Reference 32 under the Creative Commons Attribution 4.0 International license. (b) Schematic illustration of the electrical double layer on the carbon surface without and with CTAB from Reference 32 under the Creative Commons Attribution 4.0 International license. (c) Schematic illustration of 2e$^-$ ORR with/without Na^+. Reprinted with permission from Reference 34. (d) H_2O_2 FE% of

carbon black in 0.1M H_2SO_4 with/without Na^+ in 0.1M H_2SO_4. Reprinted with permission from Reference 34. (e) Illustration of the hydrophobic ($-CF_3$) and hydrophilic ($-SO_3^-$) motifs seen in Nafion on copper catalyst supported on Gas diffusion electrode. Reprinted with permission from Reference 35.

Other works involving reductive reactions, such as the CO_2 reduction reaction, have explored limiting proton availability on the catalyst surface via the addition of perfluorinated sulfonic acid (PFSA) binders such as Nafion.[35,36] PFSA binders consist of a long hydrophobic poly(tetrafluoroethylene) (PTFE) backbone with repeating hydrophilic sulfonic acid side chains. García de Arquer et al coated a copper catalyst with Nafion to create a microenvironment that limited the availability of protons on the catalyst surface.[35] This dramatically improved the performance of the copper catalysts, with the coated catalysts reaching a CO_2 reduction current of 800mA cm^{-2} compared to the bare copper catalyst peaking at 50 mA cm^{-2} before a majority of the current went towards HER. This paper introduces binder choice as a strategy to influence proton availability on the surface of the catalyst.

1.4 Direct Electrochemical Oxidation of 1,4 Dioxane

As mentioned in Section 1.1, an AOP refers to an advanced oxidation process that results in the formation of ROS, mainly hydroxyl radicals.[1] An electrochemical AOP utilizes electrochemical techniques to achieve the production of the oxidizing species, which can be classified into indirect and direct, as shown in

Figure 1-4**a**.[9,37] In an indirect electrochemical AOP such as the EF process, hydroxyl radicals are formed through secondary reactions in solution instead of on the electrode surface.[38] Most work

done for electrochemical 1,4-dioxane degradation focuses on direct processes, where water molecules are oxidized to produce hydroxyl radicals directly on the anode.[10–13] This mechanism is well-established and occurs on metal oxides (MO_x), creating hydroxyl radicals via the water oxidation reaction (WOR) pathway, as shown in **Eq 4**.[38,39] The adsorbed radicals can then oxidize the organic contaminant on the catalyst surface (**Eq 5**). These radicals may also be further oxidized to produce chemisorbed oxygen (**Eq 6**) or oxygen evolution (**Eq 7**). The chemisorbed oxygen can produce either molecular oxygen (**Eq 8**) or act as an oxidizing agent (**Eq 9**).

$$MO_x + H_2O \rightarrow MO_x(HO^\bullet) + e^- + H^+ \quad (4)$$

$$MO_x(HO^\bullet) + RH \rightarrow MO_x + H_2O + R^\bullet \quad (5)$$

$$MO_x(HO^\bullet) \rightarrow MO_{x+1} + e^- + H^+ \quad (6)$$

$$MO_x(HO^\bullet) \rightarrow MO_x + e^- + H^+ + 0.5\,O_2 \quad (7)$$

$$MO_{x+1} \rightarrow MO_x + 0.5\,O_2 \quad (8)$$

$$MO_{x+1} + RH \rightarrow MO_x + RHO \quad (9)$$

Catalyst materials for anodic electrochemical oxidation are categorized into two groups: active and inactive.[39,40] Active anodes exhibit low oxygen evolution overpotentials and a tendency for the chemisorption of hydroxyl radicals, making them good electrocatalysts for OER.[40] However, the strong binding between these catalysts and adsorbed intermediates (such as adsorbed oxygen or hydroxyl radicals) makes them less suited for direct electrochemical oxidation. In contrast, non-active materials have weaker binding to the oxygen intermediates, leading to lower OER activity but higher activity for direct electrochemical oxidation. This trend in binding strengths is also observed in selecting materials for $2e^-$ WOR to H_2O_2, as seen in **Figure 1-4c**.[20,41,42] Catalysts with higher

binding energies for adsorbed oxygen species are also effective electrocatalysts for $2e^-$ WOR as they exhibit sufficiently weak binding to discourage OER.[41] Therefore, when exploring alternatives to the expensive BDD electrode for direct electrooxidation, it's reasonable to consider materials that also show selectivity towards $2e^-$ WOR to H_2O_2.

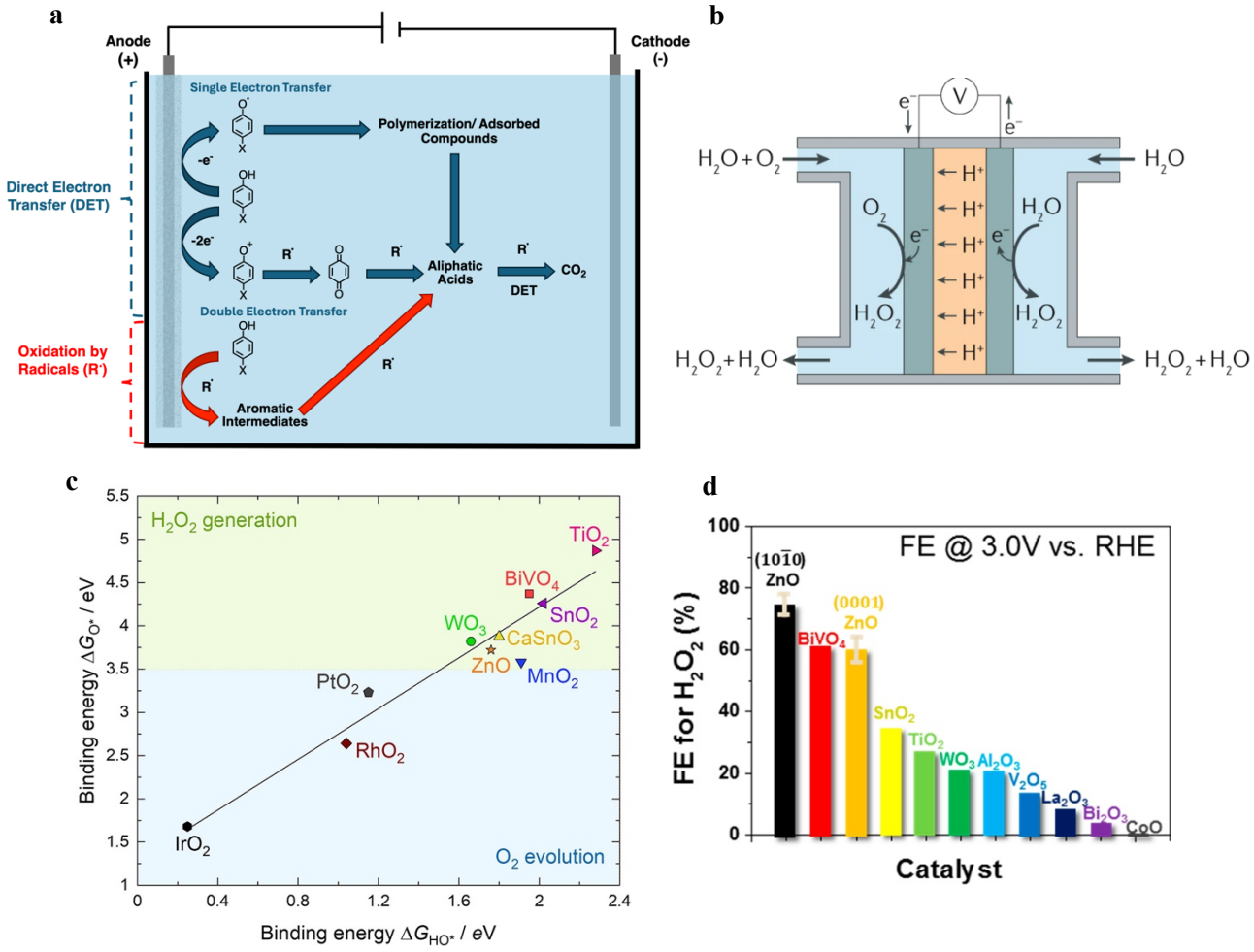


Figure 1-4- (a) Schematic illustration of direct and indirect electrochemical anodic-oxidation pathways for organic compounds. Adapted with permission from Reference 9 (b) Schematic of

flow cell producing H_2O_2 on both cathode and anode through ORR and WOR, respectively. Reproduced with permission from Reference 20 (c) Selectivity diagram for WOR to H_2O_2 on various metal oxides. Reproduced with permission from Reference 41 (d) H_2O_2 FE% for various metal oxides at 3.0 V vs RHE. Reproduced with permission Reference 43.

As mentioned earlier in this section, catalyst selectivity towards $2e^-$ WOR is heavily dependent on the material's binding strength to adsorbed oxygen intermediates. In a study done by Kelly et al., they created a volcano plot that related the limiting reaction potential to $^*OH$ binding free energies of different facets of ZnO to known catalysts. [43] Based on DFT studies and experimental work, it was found that $(10\bar{1}0)$ ZnO had the highest H_2O_2 FE% out of known metal oxides (as seen in **Figure 1-4d**). ZnO is also easily accessible, cheap, and non-toxic, making it a suitable material for use in a wastewater treatment system.

1.5 Scope of Thesis

This thesis describes a rational design for an electrochemical system that oxidizes dioxane both directly (through anodic oxidation) and indirectly (through the EF process), determining how parameters such as iron concentration, potential, and electrolyte affect product selectivity. **Chapter 1** provides the motivation for this thesis. **Chapter 2** describes the methods used in these experiments. **Chapter 3** focuses on the optimization of hydrogen peroxide generation on the cathode via catalyst design and electrolyte composition. **Chapter 4** investigates how the electrochemical parameters, such as iron concentration, potential, and electrolyte, affect product selectivity of direct and indirect dioxane oxidation.

Chapter 2

Methods and Materials

2.1 Catalyst Fabrication

2.1.1 Fabrication of PFSA:CB (5% w/w) Cathode

The 5% PFSA:CB catalyst ink was prepared by mixing 10 mg Vulcan Carbon Black (Fuel Cell Store) with 0.8856mL of a 4:1 Reagent Alcohol (Sigma Aldrich, <0.003% water): deionized water mixture. The mixture was sonicated for a few seconds to disperse the powder in the solvent. Once dispersed, 0.114mL of a PFSA Dispersion D5 solution (Fuel Cell Store, ~5% in a mixture of lower aliphatic alcohols) diluted 10x in reagent alcohol was added to the mixture. The ink mixture was then sonicated for 1h in a closed centrifuge tube. Once evenly dispersed, 20mL of the catalyst was deposited onto a 0.5cm^2 piece of carbon paper (CB) (Toray 60 Carbon paper, Fuel Cell Store) and spread using the pipette tip to form an even layer. This layer was left to air dry for 15 minutes before repeating the deposition steps twice more to result in three layers overall with a total catalyst material deposition of 0.6mg/cm^{-2}.

2.1.2 Electrodeposition of ZnO Anode

The electrodeposited ZnO electrode was fabricated using an adapted procedure from Yoshida et al.[44] Substrates were made by cutting Toray paper into a 1cm by 2cm piece with an extra 0.5cm^2 portion left for attaching to the electrode holder. The deposition solution consisted of a 0.1M Zinc acetate with 0.5M KNO_3 solution heated to 80ºC. The substrate was then connected to the potentiostat

as a cathode, with a Pt mesh acting as the anode and a double junction Ag/AgCl reference electrode. Deposition was carried out by applying a cathodic current of 20mA/cm^{-2} to a total charge passed of 20C/cm^{-2}. After deposition, each electrode was gently rinsed with deionized water and left in deionized water heated to 80^{o}C for 20 minutes. They were then left to air dry overnight.

2.2 Catalyst Characterization

2.2.1 X-ray Diffraction Analysis (XRD)

Powder XRD patterns of ZnO catalyst supported on carbon paper were collected on a Malvern Panalytical Aeris Benchtop XRD at r.t. operating at 40kV. The instrument was equipped with a copper anode. The incident beam was collimated by a 1.52mm divergence slit.

2.2.2 Electrochemical Assessment

The activity of the 5% PFSA:CB catalyst towards ORR was evaluated in 0.5M Na_2SO_4 (Sigma Aldrich, >99%) diluted in deionized water at pH 3 using H_2SO_4 (Sigma Aldrich, 95-98%). All Cyclic Voltammetry (CV) was performed in an undivided three-electrode cell with a single junction Ag/AgCl (3.5M KCl) reference electrode and Pt mesh counter electrode. The CV cycles ranged from 0.7V to -1.1V at 10mV/s for 10 scans. The activity of the ZnO catalyst toward WOR on carbon paper was also assessed in an identical set-up, using 2M $KHCO_3$ as the electrolyte. The CV cycles ranged from 0.15V to 2.5V at 10mV/s for 10 scans.

Potentials were converted to V vs RHE using the equation **Error! Reference source not found.**.

$$E_{RHE} = E^{o}_{Ag/AgCl,3.5M\ KCl} + \mathrm{E}_{Ag/AgCl,\ 3.5\mathrm{M\ KCl}} + 0.059pH \qquad (10)$$

2.3 Product Identification and Quantification

2.3.1 Nuclear Magnetic Resonance Spectroscopy (NMR)

Non-ionic products and dioxane were quantified using ^{1}H NMR (Bruker 300MHz) of crude reaction mixtures spiked with maleic acid (Sigma Aldrich, >99%) as an internal standard. The reaction products were identified using standards diluted in the corresponding electrolyte. Nuclear magnetic resonance (NMR) spectra of these products can be found in Supplementary Information. The concentration of analytes was determined using the following equation:

$$C_A = C_S \times \frac{I_A}{I_S} \times \frac{H_S}{H_A} \tag{11}$$

Where *C* represents concentration, *I* represents signal integral, and *H* represents the number of protons giving the signal of interest. *A* and *S* represent analyte and standard, respectively.

2.3.2 Ion Chromatography (IC)

Ionic products such as carboxylic acids were determined by ion chromatography (IC) using Metrohm Eco IC equipped with an anion column using 1.7mM Na_2CO_3 (ACS reagent, 99%, Sigma Aldrich) + 1.7mM $NaHCO_3$ (Sigma Aldrich, 99%) solution in Milli-Q water as an eluent.

2.3.3 UV-Vis Spectroscopy

UV-visible spectra were acquired using a deuterium-halogen light source (Ocean Optics DH-2000-BAL) and an Ocean Optics Flame-S-XR1-ES detector in a 1cm quartz cuvette. H_2O_2 quantification using $TiOSO_4$ was adapted from a procedure by Pashkova et al.[45] A stock solution of $TiOSO_4$ was made by diluting a 15wt. % $TiOSO_4$ solution (Sigma Aldrich, >99.99%) 10x in 2M H_2SO_4. Once

combined with H_2O_2 (Sigma Aldrich, 30%wt) in acidic media, $TiOSO_4$ is oxidized to form a yellow-orange peroxotitanium complex that can be quantified by UV-Vis at 409nm. Seven standards of known concentrations of the H_2O_2/$TiOSO_4$ were made and used to create a calibration curve which can be found in Appendix A.

2.3.4 Gas Chromatography (GC)

CO_2 production during the course of electrolysis was analyzed by in-line gas chromatography (GC) using an Agilent 7890B GC System.

Chapter 3

Experimental Results

3.1 Dioxane Oxidation Through Electro-Fenton Reaction

3.1.1 H_2O_2 Production on 5% Nafion:CB Catalyst in Acidic Media

As discussed in Section 1.3, one strategy for maintaining high H_2O_2 FE% selectivity on carbon materials in acidic conditions is to reduce proton concentration in the catalysts' microenvironment, thereby promoting $2e^-$ ORR over $4e^-$ ORR or HER.[32,34] Previous studies employing this strategy have utilized surfactants or cations to prevent the accumulation of protons on the catalyst surface.[32,34] However, research into other reductive reactions, such as CO_2 reduction, has investigated the use of Nafion, a commonly used PFSA binder, as a means to limit protons on the catalyst surface.[35]

Inspired by these findings, we explored the potential capabilities of PFSA binder to modulate the microenvironment of carbon black (CB) towards the $2e^-$ ORR pathway by limiting proton availability on the catalyst surface. To investigate this concept, we compared the H_2O_2 FE% of two electrodes- one containing PFSA binder and the other without- after electrolysis in a 0.5M Na_2SO_4 solution at pH 3 as seen in **Figure 3-1a** and **b**, even as little as 5% PFSA (w/w) can tailor the catalyst towards H_2O_2, with <90% FE% at current densities up to 58mA/cm^{-2}. In contrast, the catalyst without PFSA binders reached a maximum H_2O_2 FE% of 50% at a current density of 5.5mA/cm^{-2}. Additional experiments demonstrated that varying the cation concentration also influences the PFSA binder's ability to tune the microenvironment, resulting in varying selectivity toward H_2O_2 generation. A schematic illustration of the proposed mechanism is shown in **Figure 3-1c**, where the sulphate end

groups of the binder may facilitate a shielding effect using cations in the electric double layer on the catalyst surface, preventing the catalyst surface from accumulating protons.[34]

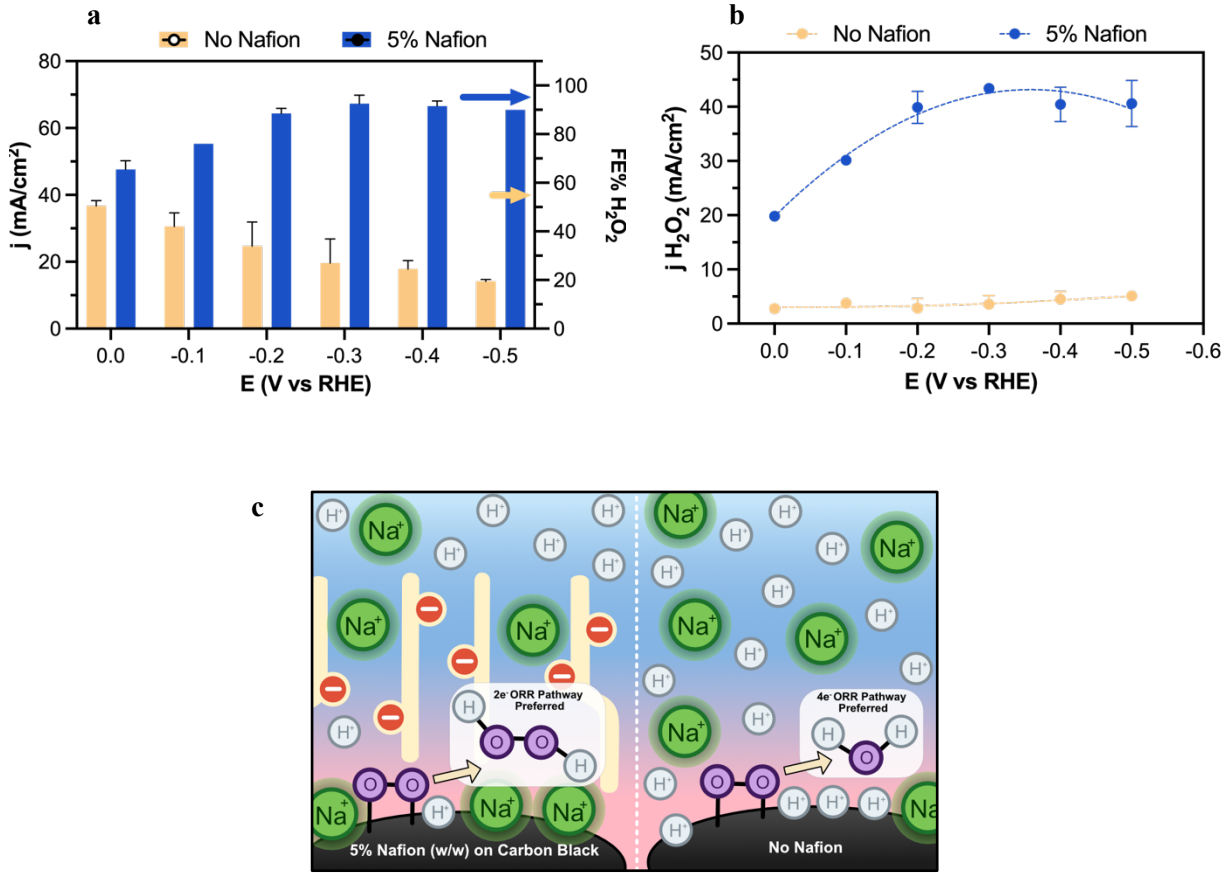


Figure 3-1 FE% of H_2O_2 (a) and $j_{H_2O_2}$ (b) as a function of potential in 0.5M Na_2SO4 at pH 3 using 5% PFSA:CB and a carbon black-based electrode with no PFSA binder. (c) Schematic illustration of increased H_2O_2 selectivity through PFSA limiting proton availability. The negatively charged sulphate end group motifs direct both proton and cations on the electrode surface, limiting adsorbed protons available for ORR and pushing reaction conditions towards $2e^-$ ORR.

To investigate the effect of cations on H_2O_2 generation using a 5% PFSA:CB catalyst in acidic media, a two-cell compartment setup separated by a proton exchange membrane (Nafion) was employed. The solution was brought to pH 3 using H_2SO_4, allowing for one to examine the potential shielding effect while minimizing the presence of excess protons in the solution at lower Na_2SO_4 concentrations. The electrochemical behaviour of the carbon catalysts, both with and without PFSA, was initially assessed through cyclic voltammetry (**Figure 3-2**) in O_2- or Ar-saturated 0.5M Na_2SO_4. The onset potential for the catalyst was found to be 0.2V vs. RHE, which aligns with previously reported values.[51] After identifying an appropriate range of reductive potentials for analysis, a series of potentiostatic electrolysis experiments were conducted in O_2-saturated Na_2SO_4 solutions with concentrations ranging from 0.025M to 0.5M at pH 3. The reactions were terminated after passing 10C, and the concentration of H_2O_2 in the solution was determined via UV-Vis quantification of H_2O_2 reaction with $TiOSO_4$.

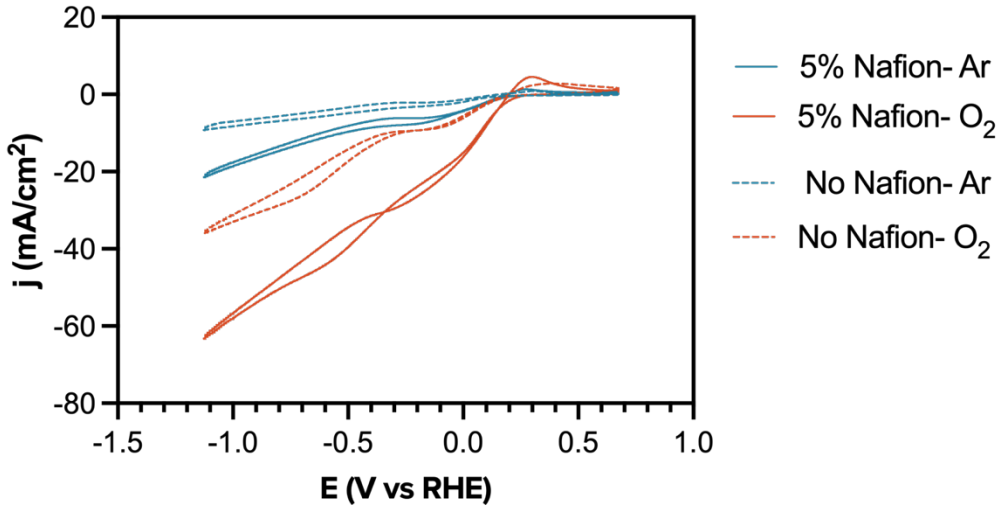


Figure 3-2- Cyclic Voltammetry of CB catalyst with and without PFSA binder in 0.5M Na_2SO_4 at pH 3 using H_2SO_4

As illustrated in **Figure 3-3**, the primary product of the ORR at any tested potential is H_2O_2, showcasing carbon's selectivity towards $2e^-$ ORR. The FE% for H_2O_2 was found to be highest and lowest at a Na_2SO_4 concentration of 0.5M (93% at -0.2V and 65% at -0.5 V, respectively). At a Na_2SO_4 concentration of 0.025M, the FE increased slightly with more negative potential. In contrast, in 0.5M Na_2SO_4, the H_2O_2 FE% peaked at 93% before decreasing steadily with increasing applied potential. This trend suggests that, at the current carbon to Nafion ratio, the cation shielding effect is limited in its ability to protect the catalyst surface from increasing proton concentration on the catalyst surface at more reductive potentials.

At lower Na_2SO_4 concentrations, such as 0.025M, the initial Na^+ cations concentration on the catalyst surface is low but grows with increasing applied potential. This results in a higher selectivity towards H_2O_2 FE% with more negative potentials due to the growing shielding effect. At 0.05M Na_2SO_4, the initial local cation concentration is sufficient to generate a shielding effect, even at less negative potentials, resulting in high H_2O_2 FE% that decreases slightly with increasing applied potential as the shielding effect is still limited in its effectiveness. The limitations of the shielding effect become even more pronounced, with 0.5M Na_2SO_4 exhibiting the highest H_2O_2 FE% (93% at -0.2V) but as the potential is further decreased, there is a steady decrease in FE% due to increasing competition from $4e^-$ ORR and HER. Despite this, the cation shielding effect at 0.5M Na_2SO_4 results in a higher $j_{H_2O_2}$ compared to lower concentrations, as shown in **Figure 3-3b** and **c**, indicating that increased cation concentration enhances H_2O_2 production.

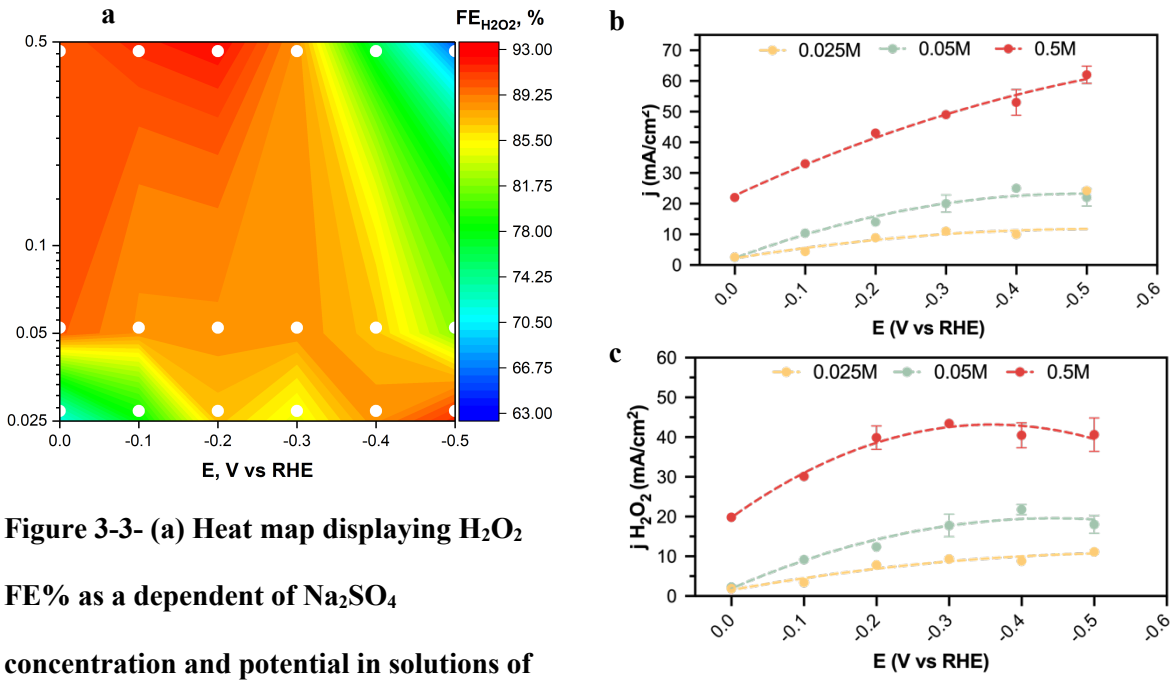


Figure 3-3- (a) Heat map displaying H_2O_2 FE% as a dependent of Na_2SO_4 concentration and potential in solutions of pH 3 using H_2SO_4. Current densities (b) and j_{H2O2} (c) as a function of potential in varying concentrations of Na_2SO_4 at pH 3 using 5% PFSA:CB.

To assess the extent of the Na^+ cation shielding effect on carbon black modified with PFSA binder, electrolysis was conducted using the same cell configuration as previously described, up to 20C has passed, using solutions of 0.5M Na_2SO_4 at varying pH levels using H_2SO_4. As illustrated in **Figure 3-4a**, an increase in pH from 1 to 3 results in a broader potential range over which the H_2O_2 FE% exceeds 90%. This observation is consistent with findings from other studies.[26] With each unit decrease in pH, the proton concentration increases by an order of magnitude. In solutions with pH 2 or 3, the PFSA binder effectively limits proton concentration at the catalyst surface, thereby expanding the range of potentials at which H_2O_2 FE% remains high (>90%). However, at pH 1, the binder's ability to mitigate proton availability at the catalyst surface is less pronounced, leading to increased competition from the $4e^-$ ORR pathway and HER.

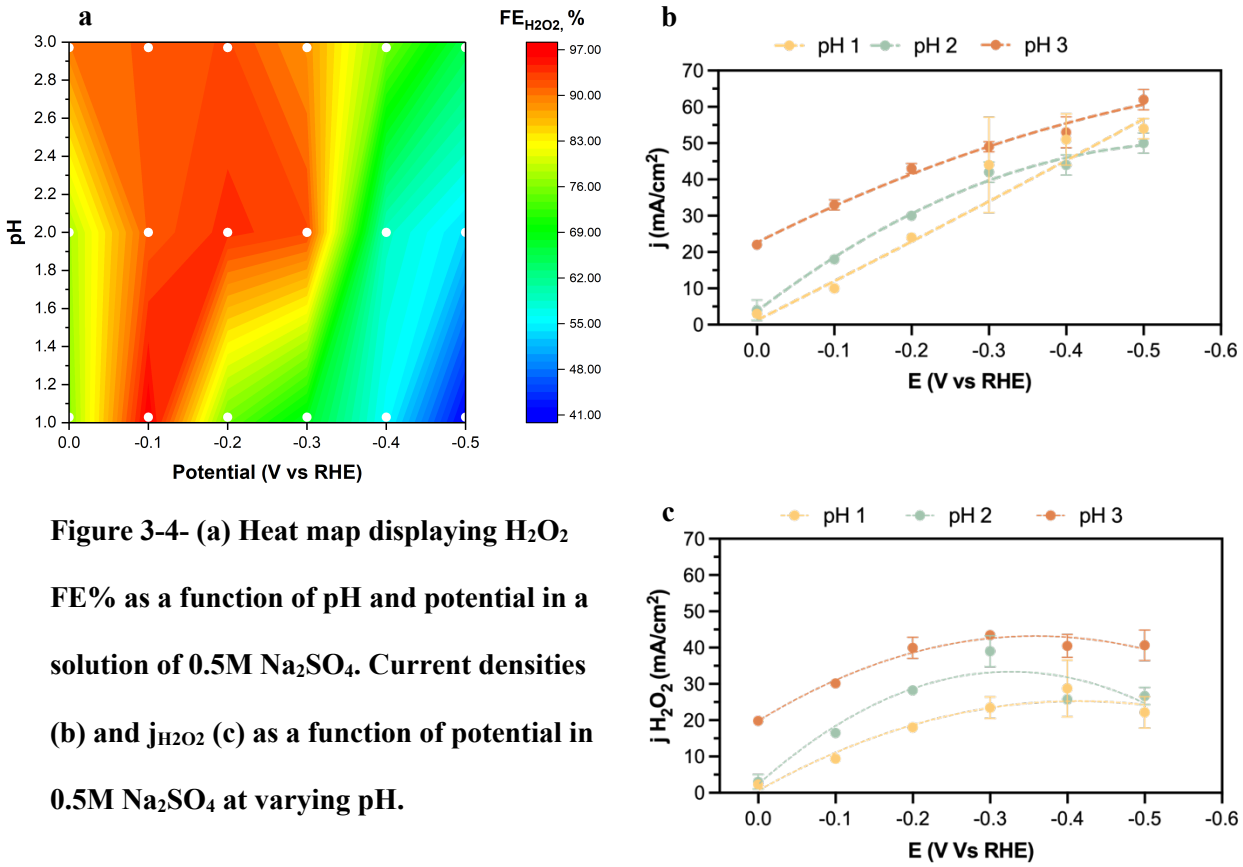


Figure 3-4- (a) Heat map displaying H_2O_2 FE% as a function of pH and potential in a solution of 0.5M Na_2SO_4. Current densities (b) and j_{H2O2} (c) as a function of potential in 0.5M Na_2SO_4 at varying pH.

While short-term H_2O_2 FE% is a valuable parameter for characterizing a catalyst's activity toward the $2e^-$ oxygen reduction reaction (ORR), it is crucial to test whether the catalyst can accumulate H_2O_2 in the bulk solution rather than further reduce it to H_2O. To determine whether the PFSA binder would aid in maintaining high H_2O_2 FE%, long-term electrolysis was performed in a flow cell in an O_2-saturated 0.5M Na_2SO_4 solution at an applied potential of -0.3V (where FE% remained ≥ 90%, and the current density was above 10mA/cm^{-2}, according to **Figure 3-4b and c**) with a flow of 20 mL/min.

The FE% and H_2O_2 production rates for the two catalysts -carbon black with and without PFSA binder- are shown in **Figure 3-5a** and **b**. The catalyst with PFSA exhibited a higher current density

throughout the eight-hour experiment (40mA/cm^{-2} compared to 24mA/cm^{-2}) while maintaining a H_2O_2 FE% of approximately 93%). This indicates that not only is H_2O_2 being produced at high FE%, but the catalyst also preferentially reduces O_2 over H_2O_2, leading to a stable H_2O_2 production rate, as shown in **Figure 3-5b**. When compared to other 2e$^-$ ORR catalysts, carbon black with PFSA binders (under tailored reaction conditions that limit proton availability) achieves higher H_2O_2 production in acidic conditions at greater current densities than previously reported for other catalysts, as illustrated in **Figure 3-5c**.

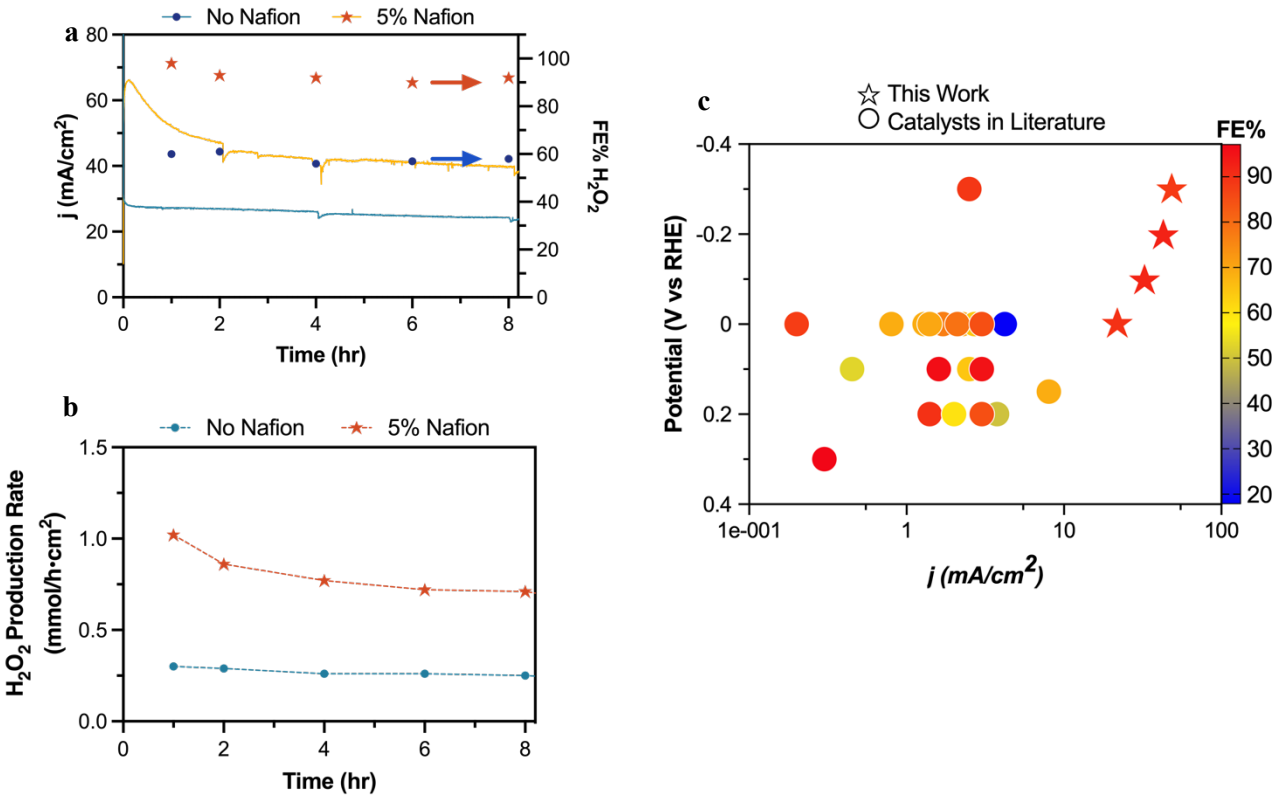


Figure 3-5- (a) CA of ORR at -0.3V in 0.5 M Na_2SO_4 electrolyte with pH 3. Symbols are used to denote H_2O_2 FE% for both catalysts: with and without PFSA binder. (b) H_2O_2 production rate

for both catalysts during the eight-hour electrolysis. (c) Comparison of 5% PFSA:CB to other catalysts in literature. The full chart can be found in Supporting information. (Table 4)

3.1.2 Products of Dioxane Oxidation as a Factor of Fe^{2+} Concentration

Once the cathode material was characterized, work began on exploring the impact of Fe^{2+} on dioxane conversion and product selectivity. This was done using a two-cell configuration in which the cathodic chamber was filled with 0.1M 1,4-dioxane using 0.5M Na_2SO_4 at pH 3 as an electrolyte. The anodic chamber was filled with 0.1M H_2SO_4 to facilitate proton transfer across the Nafion membrane. Electrolysis was performed until a charge of 500C was passed, under stirring. Previous work by Jasmann et al., proposed a reaction pathway using intermediate products observed during the direct electrochemical oxidation of dioxane by hydroxyl radicals.[10] Product standards for NMR and IC were made according to this list of potential products (can be found in **Figure 0-2**).

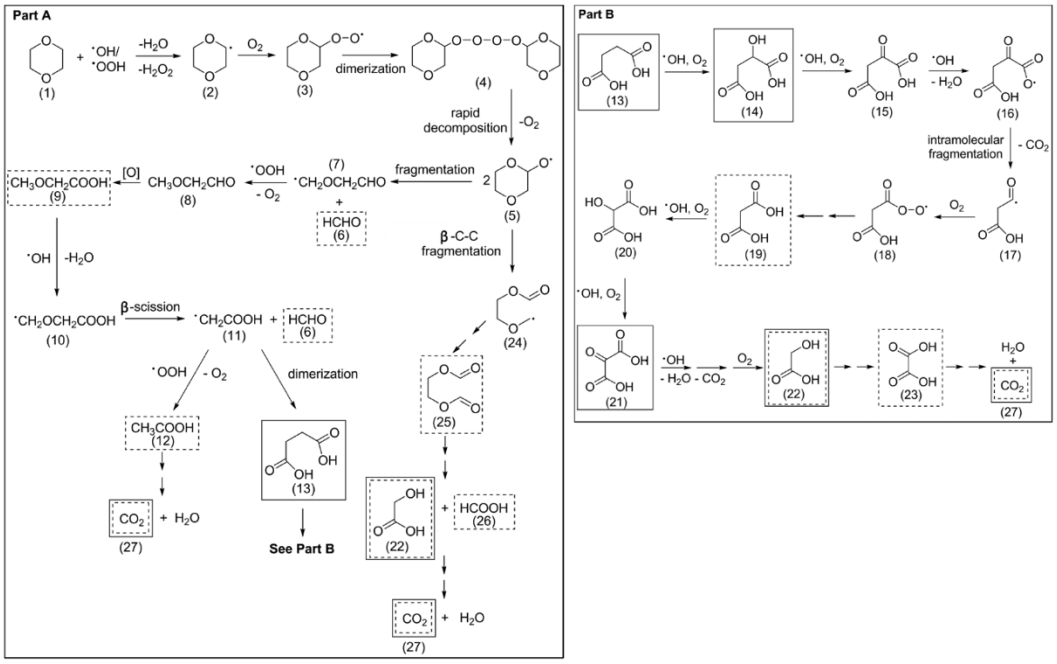


Figure 3-6: Reaction pathway for direct oxidation of dioxane, as proposed by Jasmann et al. Reproduced with permission from Reference 10.

As shown in Error! Reference source not found.**a** and **b**, with no Fe^{2+}in solution, dioxane oxidation is negligible, and product formation is low. Once Fe^{2+} is introduced into the solution, dioxane conversion increases, with conversion (%) peaking at 5mM Fe^{2+}. Both 1mM and 2mM Fe^{2+} show slightly lower conversion than no Fe to Error! Reference source not found.**a**. This could be due to most of the Fe^{2+} cations being adsorbed onto the catalyst surface instead of remaining in the bulk solution to activate H_2O_2. The adsorbed Fe^{2+} block active sites for H_2O_2 generation, resulting in lowered H_2O_2 generation, as seen in Error! Reference source not found.**b**. Once higher [Fe^{2+}] is utilized, however, we see a rise in dioxane conversion, showing that the EF process is effective at oxidizing dioxane at higher rates than using only H_2O_2 in solution. At 7mM Fe^{2+}, the concentration of

Fe^{2+} is too high, resulting in the rise of two competing reactions: Fe^{2+} cations reaction with hydroxyl radicals (**Eq 12**) and the decomposition of H_2O_2 catalyzed by excess Fe^{3+} cations (**Eq 13 and 14**).[46,47]

$$Fe^{2+} + {}^{\bullet}OH \rightarrow Fe^{3+} + OH^{-} \quad (12)$$

$$Fe^{3+} + H_2O_2 \rightarrow Fe^{3+} + {}^{\bullet}OOH + H^{+} \quad (13)$$

$$Fe^{3+} + {}^{\bullet}OOH \rightarrow Fe^{2+} + O_2 + H^{+} \quad (14)$$

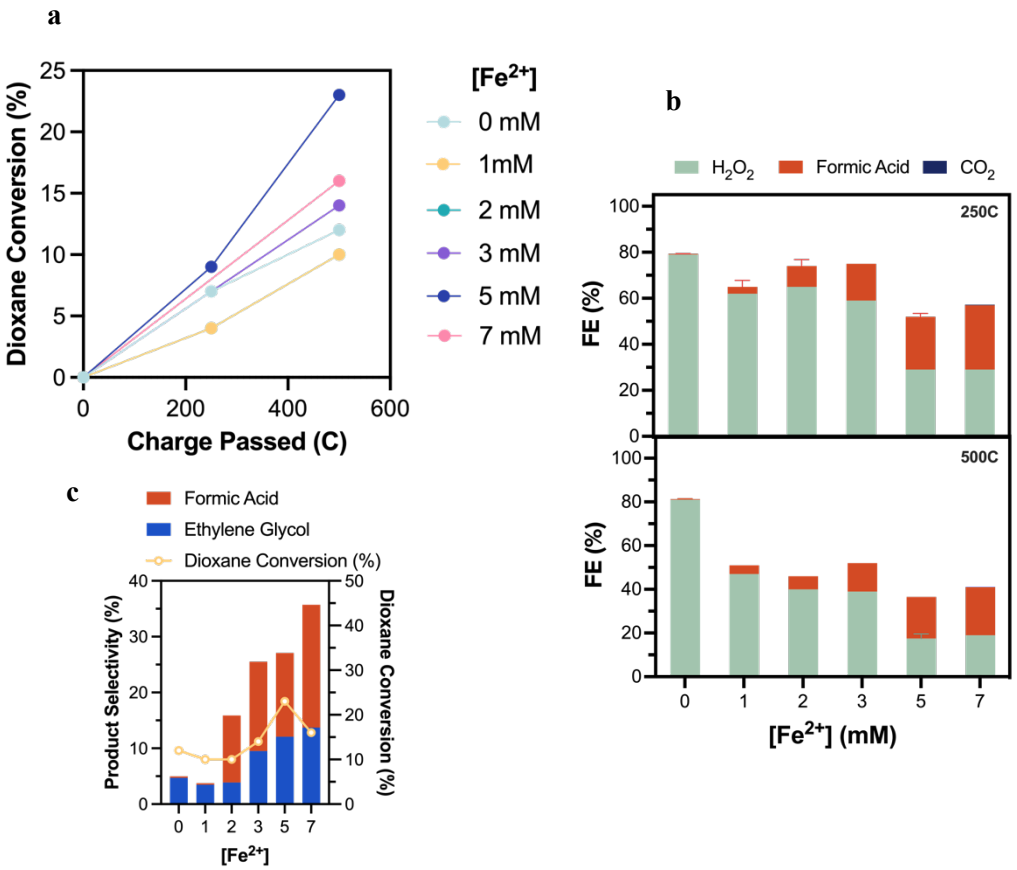


Figure 3-7- (a) Dioxane conversion as a function of Fe^{2+} concentration after passing 500 C through the carbon electrode. (b) FE% of products, including H_2O_2, formed in the cathodic

compartment after passing 250C and 500C. (c) Dioxane conversion (%) and product selectivity (%) of EF-facilitated dioxane oxidation after 500C has passed.

Upon examining the product selectivity during dioxane conversion using the EF process, it became evident that some products remain unidentified, as selectivity is significantly below 100%. This is particularly noticeable when comparing NMR spectra and IC results, as shown in **Figure 0-3** and **Figure 0-4**. Initially, CO_2 was suspected to be the missing product. However, upon GC-MS analysis, it was found that CO_2 FE% was below 1%, indicating that CO_2 is not produced in sufficient quantities to account for the unidentified products. IC analysis revealed no other ionic products besides formate, suggesting the product may be an aldehyde or alcohol, as proposed in **Figure 3-6**. Further work will be done using GC-MS to identify the unknown products and continue characterizing dioxane oxidation using EF.

3.2 Dioxane Oxidation on ZnO in Alkaline Media

3.2.1 The activity of ZnO Catalyst Towards $2e^-$ WOR

The focus of this project is to evaluate how electrochemical parameters affect the product selectivity and efficiency of electrochemical dioxane oxidation. While the EF process provides the necessary ROS indirectly, the following section examines how ZnO is capable of directly forming hydroxyl radicals dioxane conversion. The first step of this process is to ensure the deposition method mentioned in Section 0 resulted in the formation of ZnO on the carbon paper substrate. As shown in **Figure 3-8**, XRD analysis revealed the procedure resulted in ZnO depositing onto the substrate. Aluminum was also used as a reference to identify background noise from the Al sample holder.

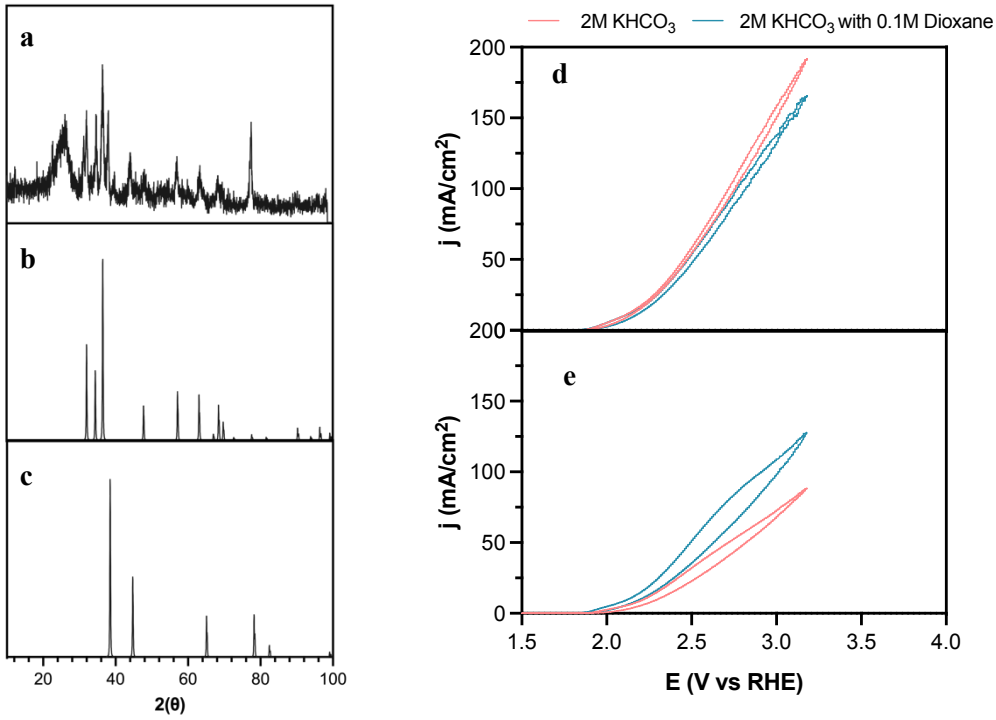


Figure 3-8- XRD analysis of (a) electrodeposited ZnO onto carbon paper substrate with (b) ZnO and (c) Aluminum as reference. Cyclic voltammetry was performed for (d) ZnO in 2M $KHCO_3$ - with and without dioxane- with (e) CB as a control.

After confirming that the catalyst material was indeed ZnO, cyclic voltammetry was used to confirm the metal oxide is capable of oxidizing dioxane. Electrolysis was conducted in an undivided cell using 2M $KHCO_3$ with and without dioxane. CB was used as a control. As shown in **Figure 3-8d** and **e** , although ZnO doesn't improve the onset of WOR, there is a peak that appears to correlate with dioxane oxidation on ZnO, a feature not observed when performing electrolysis with carbon paper This suggests ZnO can produce radicals for the electrochemical oxidation of dioxane.

3.2.2 Product Selectivity as A Factor of Potential

To evaluate dioxane oxidation on ZnO, electrolysis was performed under stirring in a two-cell compartment with a Nafion membrane. The anodic chamber was filled with 0.1M 1,4-dioxane in 2M $KHCO_3$ and the cathodic compartment was filled with 0.1M H_2SO_4 and a Pt counter electrode Once set-up was complete, electrolysis was done under four applied potentials: 2.1V, 2.2V, 2.3V, and 2.4V. It was found that 2.1V had the highest dioxane conversion (%) of 37% at 500C passed (**Figure 3-9a**). At more positive potentials, the dioxane conversion remains steady at ~14%. This could be due to $4e^-$ WOR being preferred at higher potentials, resulting in fewer ROS species available for dioxane oxidation. This was supported by the appearance of bubbles on the anode at potentials higher than 2.3V, signalling OER is occurring.

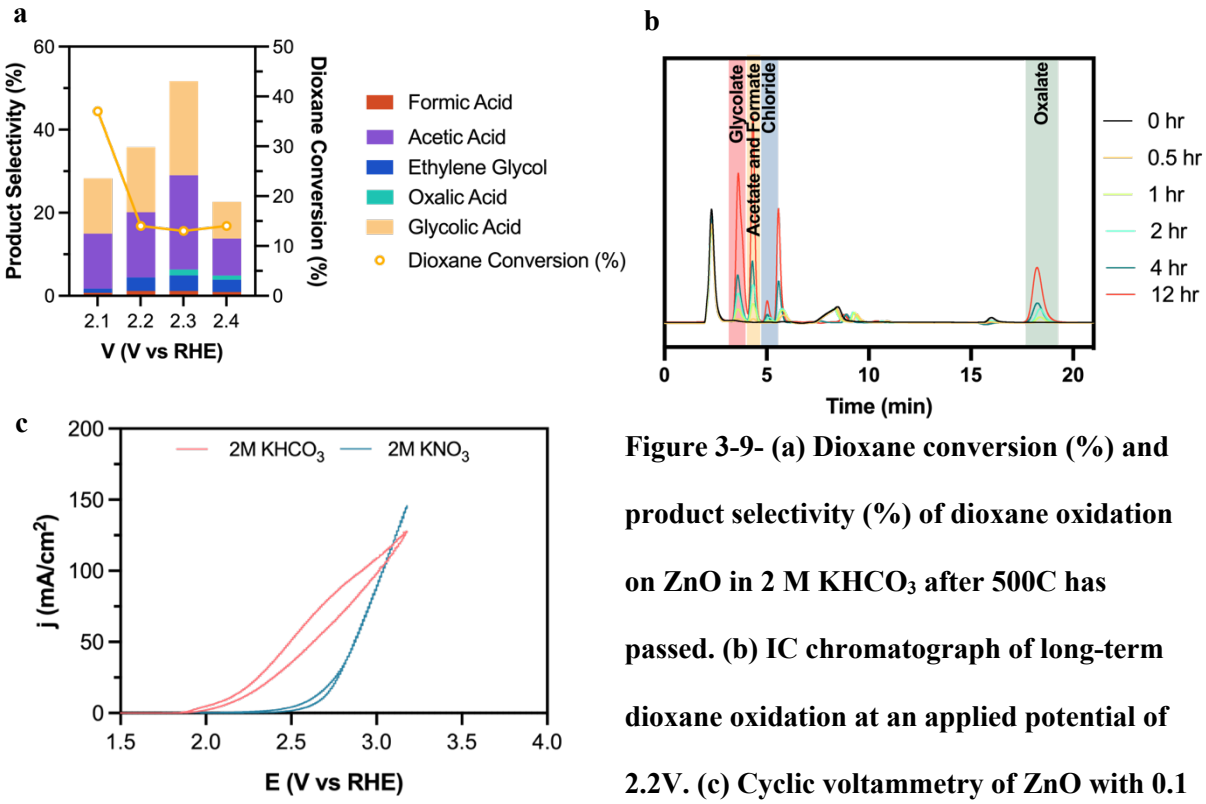


Figure 3-9- (a) Dioxane conversion (%) and product selectivity (%) of dioxane oxidation on ZnO in 2 M $KHCO_3$ after 500C has passed. (b) IC chromatograph of long-term dioxane oxidation at an applied potential of 2.2V. (c) Cyclic voltammetry of ZnO with 0.1 M dioxane in 2M $KHCO_3$ (red) and 2M KNO_3 (blue).

The anodic oxidation of dioxane shows a wider breadth of carboxylic acids as products than the EF process, with glycolic acid and acetic acid being the major products at all tested potentials. However, not all the products have been accounted for, as seen when calculating product selectivity (%) in **Figure 3-9a.** Unlike with the cathodic reaction, CO_2 cannot be ignored as a possible product as it is not possible to differentiate CO_2 produced from dioxane oxidation from that which is produced from the saturated $KHCO_3$ electrolyte using GC-MS. However, the increase in the variety of liquid products, as seen in **Figure 3-9b**, suggests that the unknown products are not gaseous. When comparing ^1H NMR peaks of known products of dioxane oxidation via hydroxyl radicals to those appearing in the spectra, it was found that a few peaks did not match known standards, implying dioxane oxidation may occur through a different pathway. Upon further investigation, it was found that hydrogen peroxide generation through WOR on most materials occurs via a carbonate-mediated pathway as opposed to the formation of hydroxyl radicals.[48] This pathway results in the formation of a carbonate radical, which is less indiscriminate in reaction sites than hydroxyl radicals.[49] To determine whether this pathway may be responsible for anodic dioxane oxidation on ZnO , cyclic voltammetry was performed in 0.1M dioxane diluted in 2M KNO_3. As seen in **Figure 3-9c** , there is no peak to dioxane oxidation in the KNO_3 electrolyte, as opposed to in $KHCO_3$. The onset for WOR In 2M $KHCO_3$ is also much lower than that of KNO_3 (2.1V vs 2.7V), indicating a change in the mechanism for WOR. Further work will be done using GC-MS to identify the unknown products.

Chapter 4

Conclusions and Outlook

In this work, we aimed to create a system for the simultaneous treatment for 1,4-dioxane on the cathode and anode via indirect and direct AOPs. By providing a systematic analysis of the electrochemical parameters that affect product selectivity and dioxane conversion, it's possible to tailor oxidation toward target products, thus adding value to the treatment of 1,4-dioxane.

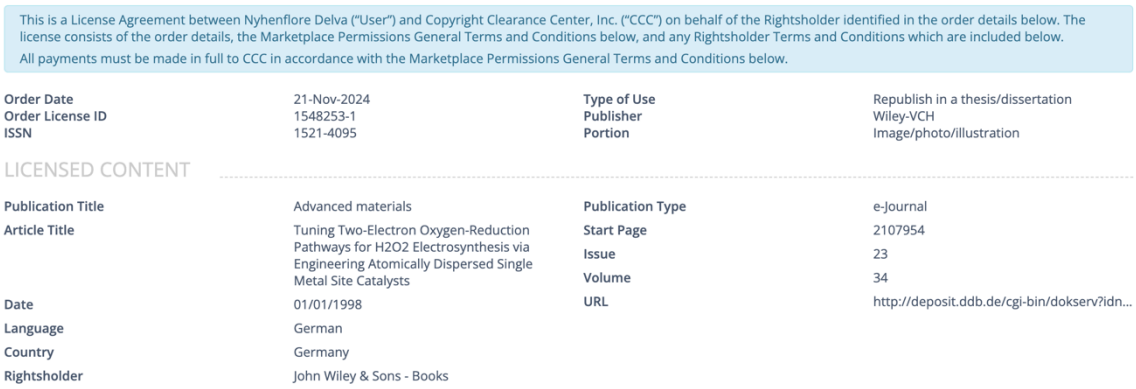
It was found that choice of binders can improve H_2O_2 selectivity by limiting proton availability on cheap carbon materials in acidic media, with as little as 5% PFSA (wt%) improving carbon black's selectivity towards H_2O_2 from 50% at 5.5mA/cm^{-2} to >90% at current densities of 58mA/cm^{-2}. Experimental data have shown that this ability to limit proton availability is also aided by increasing cation concentration in solution, by forming an electrical double layer that repels other positively charged species such as protons, from the catalyst surface. pH also affects H_2O_2 selectivity, as the range of high H_2O_2 FE% (>90%) broadens with increasing pH. Long-term experiments in a flow cell show the PFSA-modified catalyst is stable and preferentially reduces O_2 over H_2O_2, maintaining a H_2O_2 FE% of ~93% in 0.5M Na_2SO_4 at pH 3 H_2SO_4, significantly higher than the H_2O_2 FE% of unmodified carbon black which maintained a H_2O_2 FE% of ~58%

The EF process has also shown promise to tailor dioxane oxidation, with product selectivity shifting with Fe^{2+}. It has been shown that too little a concentration of Fe^{2+} results in the carbon adsorbing Fe^{2+} onto its surface, lowering its' H_2O_2 FE% and preventing the cation from activating H_2O_2. At higher Fe^{2+} concentrations, excess Fe^{3+} catalyzes the decomposition of H_2O_2. Early work discussed in Section 3.2.2 suggests that the anodic oxidation of dioxane on ZnO appears to occur

using a carbonate-mediated pathway, with early work indicating a different product range from proposed reaction pathways via hydroxyl radicals. This has the potential to expand the range of potential target compounds from electrochemical dioxane oxidation while using cheaper catalyst materials such metal oxides.

Further work will be done with the help of the Mass Spectrometry Lab at the University of Waterloo to further identify unknown products and evaluate how certain parameters affect both the direct and indirect electrochemical oxidation of dioxane.

Letters of Copyright Permission



This is a License Agreement between Nyhenflore Delva ("User") and Copyright Clearance Center, Inc. ("CCC") on behalf of the Rightsholder identified in the order details below. The license consists of the order details, the Marketplace Permissions General Terms and Conditions below, and any Rightsholder Terms and Conditions which are included below.

All payments must be made in full to CCC in accordance with the Marketplace Permissions General Terms and Conditions below.

Order Date	21-Nov-2024	**Type of Use**	Republish in a thesis/dissertation
Order License ID	1548253-1	**Publisher**	Wiley-VCH
ISSN	1521-4095	**Portion**	Image/photo/illustration

LICENSED CONTENT

Publication Title	Advanced materials	**Publication Type**	e-Journal
Article Title	Tuning Two-Electron Oxygen-Reduction Pathways for H2O2 Electrosynthesis via Engineering Atomically Dispersed Single Metal Site Catalysts	**Start Page**	2107954
		Issue	23
		Volume	34
Date	01/01/1998	**URL**	http://deposit.ddb.de/cgi-bin/dokserv?idn...
Language	German		
Country	Germany		
Rightsholder	John Wiley & Sons - Books		

Figure 1-2- Scheme of 2e- and 4e- pathways seen in electrochemical ORR. Reprinted with permission from Reference 21 under the Creative Commons Attribution 4.0 International license.

This is a License Agreement between Nyhenflore Delva ("User") and Copyright Clearance Center, Inc. ("CCC") on behalf of the Rightsholder identified in the order details below. The license consists of the order details, the Marketplace Permissions General Terms and Conditions below, and any Rightsholder Terms and Conditions which are included below.
All payments must be made in full to CCC in accordance with the Marketplace Permissions General Terms and Conditions below.

Order Date	20-Nov-2024	Type of Use	Republish in a thesis/dissertation
Order License ID	1548225-1	Publisher	Nature Publishing Group
ISSN	2041-1723	Portion	Image/photo/illustration

LICENSED CONTENT

Publication Title	Nature Communications	Publication Type	e-Journal
Article Title	Electrochemical oxygen reduction to hydrogen peroxide at practical rates in strong acidic media	Start Page	2880
		Issue	1
Date	01/01/2010	Volume	13
Language	English	URL	http://www.nature.com/ncomms/index.h...
Country	United Kingdom of Great Britain and Northern Ireland		
Rightsholder	Springer Nature BV		

This is a License Agreement between Nyhenflore Delva ("User") and Copyright Clearance Center, Inc. ("CCC") on behalf of the Rightsholder identified in the order details below. The license consists of the order details, the Marketplace Permissions General Terms and Conditions below, and any Rightsholder Terms and Conditions which are included below.
All payments must be made in full to CCC in accordance with the Marketplace Permissions General Terms and Conditions below.

Order Date	21-Nov-2024	Type of Use	Republish in a thesis/dissertation
Order License ID	1548226-1	Publisher	AMERICAN ASSOCIATION FOR THE ADVANCEMENT OF SCIENCE
ISSN	1095-9203	Portion	Image/photo/illustration

LICENSED CONTENT

Publication Title	Science	Publication Type	e-Journal
Article Title	CO2 electrolysis to multicarbon products at activities greater than 1 A cm-2.	Start Page	661
		End Page	666
Author / Editor	American Association for the Advancement of Science.	Issue	6478
		Volume	367
Date	01/01/1880	URL	http://www.sciencemag.org/archive
Language	English		
Country	United States of America		
Rightsholder	American Association for the Advancement of Science		

Figure 1-3 (a) H_2O_2 FE% of carbon black in 0.1M H_2SO_4 with the addition of CTAB. (c) Schematic illustration of $2e^-$ ORR with/without Na^+. Reprinted with permission from Reference 32. (b) Schematic illustration of the electrical double layer on the carbon surface without and with CTAB. Adapted with permission from Reference 32 (c) Schematic illustration of $2e^-$ ORR with/without Na^+. Reprinted with permission from Reference 34. (d) H_2O_2 FE% of carbon black in 0.1M H_2SO_4 with/without Na^+ in 0.1M H_2SO_4. Reprinted with permission from Reference 34 (e) Illustration of the hydrophobic ($-CF_3$) and hydrophilic ($-SO_3^-$) motifs seen in Nafion on copper catalyst supported on Gas diffusion electrode. Reprinted with permission from Reference 35.

ZnO As an Active and Selective Catalyst for Electrochemical Water Oxidation to Hydrogen Peroxide

Author: Sara R. Kelly, Xinjian Shi, Seoin Back, et al
Publication: ACS Catalysis
Publisher: American Chemical Society
Date: May 1, 2019

Copyright © 2019, American Chemical Society

PERMISSION/LICENSE IS GRANTED FOR YOUR ORDER AT NO CHARGE

This type of permission/license, instead of the standard Terms and Conditions, is sent to you because no fee is being charged for your order. Please note the following:

- Permission is granted for your request in both print and electronic formats, and translations.
- If figures and/or tables were requested, they may be adapted or used in part.
- Please print this page for your records and send a copy of it to your publisher/graduate school.
- Appropriate credit for the requested material should be given as follows: "Reprinted (adapted) with permission from {COMPLETE REFERENCE CITATION}. Copyright {YEAR} American Chemical Society." Insert appropriate information in place of the capitalized words.
- One-time permission is granted only for the use specified in your RightsLink request. No additional uses are granted (such as derivative works or other editions). For any uses, please submit a new request.

If credit is given to another source for the material you requested from RightsLink, permission must be obtained from that source.

BACK CLOSE WINDOW

Recent Advances in Electrochemical Water Oxidation to Produce Hydrogen Peroxide: A Mechanistic Perspective

Author: Sotirios Mavrikis, Samuel C. Perry, Pui Ki Leung, et al
Publication: ACS Sustainable Chemistry & Engineering
Publisher: American Chemical Society
Date: Jan 1, 2021

Copyright © 2021, American Chemical Society

PERMISSION/LICENSE IS GRANTED FOR YOUR ORDER AT NO CHARGE

This type of permission/license, instead of the standard Terms and Conditions, is sent to you because no fee is being charged for your order. Please note the following:

- Permission is granted for your request in both print and electronic formats, and translations.
- If figures and/or tables were requested, they may be adapted or used in part.
- Please print this page for your records and send a copy of it to your publisher/graduate school.
- Appropriate credit for the requested material should be given as follows: "Reprinted (adapted) with permission from {COMPLETE REFERENCE CITATION}. Copyright {YEAR} American Chemical Society." Insert appropriate information in place of the capitalized words.
- One-time permission is granted only for the use specified in your RightsLink request. No additional uses are granted (such as derivative works or other editions). For any uses, please submit a new request.

If credit is given to another source for the material you requested from RightsLink, permission must be obtained from that source.

BACK CLOSE WINDOW

This is a License Agreement between Nyhenflore Delva ("User") and Copyright Clearance Center, Inc. ("CCC") on behalf of the Rightsholder identified in the order details below. The license consists of the order details, the Marketplace Permissions General Terms and Conditions below, and any Rightsholder Terms and Conditions which are included below.

All payments must be made in full to CCC in accordance with the Marketplace Permissions General Terms and Conditions below.

Order Date	21-Nov-2024	**Type of Use**	Republish in a thesis/dissertation
Order License ID	1548229-1	**Publisher**	Nature Research
ISSN	2397-3358	**Portion**	Image/photo/illustration

LICENSED CONTENT

Publication Title	Nature Reviews Chemistry	**Publication Type**	e-Journal
Article Title	Electrochemical synthesis of hydrogen peroxide from water and oxygen	**Start Page**	442
	01/01/2017	**End Page**	458
Date	01/01/2017	**Issue**	7
Language	English	**Volume**	3
Country	United Kingdom of Great Britain and Northern Ireland	**URL**	http://www.nature.com/natrevchem
Rightsholder	Springer Nature BV		

Figure 1-4 (a) Schematic illustration of direct and indirect electrochemical anodic-oxidation pathways for organic compounds. Adapted with permission from Reference 9 (b) Schematic of flow cell producing H_2O_2 on both cathode and anode through ORR and WOR, respectively. Reproduced with permission from Reference 20 (c) Selectivity diagram for WOR to H_2O_2 on various metal oxides. Reproduced with permission from Reference 41 (d) H_2O_2 FE% for various metal oxides at 3.0 V vs RHE. Reproduced with permission Reference 43.

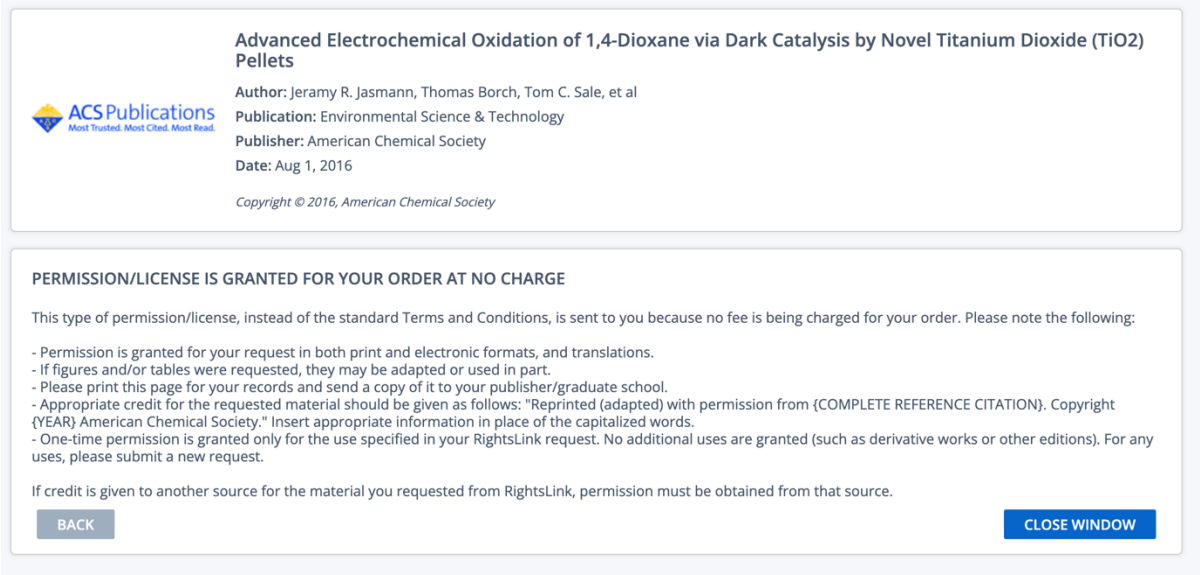


Figure 3-6: Reaction pathway for direct oxidation of dioxane, as proposed by Jasmann et al. Reproduced with permission from Reference 10.

References

(1) Tang, Y.; Mao, X. Recent Advances in 1,4-Dioxane Removal Technologies for Water and Wastewater Treatment. *Water* **2023**, *15* (8), 1535. https://doi.org/10.3390/w15081535.

(2) Tawfik, A. Degradation Pathways of 1,4-Dioxane in Biological and Advanced Oxidation Processes. *DESALINATION WATER Treat.* **2020**, *178*, 360–386. https://doi.org/10.5004/dwt.2020.24970.

(3) Kujawska, A.; Kiełkowska, U.; Atisha, A.; Yanful, E.; Kujawski, W. Comparative Analysis of Separation Methods Used for the Elimination of Pharmaceuticals and Personal Care Products (PPCPs) from Water – A Critical Review. *Sep. Purif. Technol.* **2022**, *290*, 120797. https://doi.org/10.1016/j.seppur.2022.120797.

(4) Degradation of 1,4-Dioxane by Heterogeneous Photocatalysis and a Photo-Fenton-like Process under Fluorescent Light. *Environ. Technol.* **2024**, *45* (14), 2879–2890. https://doi.org/10.1080/09593330.2023.2192367.

(5) Beckett, M. A.; Hua, I. Elucidation of the 1,4-Dioxane Decomposition Pathway at Discrete Ultrasonic Frequencies. *Environ. Sci. Technol.* **2000**, *34* (18), 3944–3953. https://doi.org/10.1021/es000928r.

(6) Stefan, M. I.; Bolton, J. R. Mechanism of the Degradation of 1,4-Dioxane in Dilute Aqueous Solution Using the UV/Hydrogen Peroxide Process. *Environ. Sci. Technol.* **1998**, *32* (11), 1588–1595. https://doi.org/10.1021/es970633m.

(7) Merayo, N.; Hermosilla, D.; Cortijo, L.; Blanco, Á. Optimization of the Fenton Treatment of 1,4-Dioxane and on-Line FTIR Monitoring of the Reaction. *J. Hazard. Mater.* **2014**, *268*, 102–109. https://doi.org/10.1016/j.jhazmat.2014.01.008.

(8) Lee, C.-S.; Venkatesan, A. K.; Walker, H. W.; Gobler, C. J. Impact of Groundwater Quality and Associated Byproduct Formation during UV/Hydrogen Peroxide Treatment of 1,4-Dioxane. *Water Res.* **2020**, *173*, 115534. https://doi.org/10.1016/j.watres.2020.115534.

(9) Zhang, J.; Zhou, Y.; Yao, B.; Yang, J.; Zhi, D. Current Progress in Electrochemical Anodic-Oxidation of Pharmaceuticals: Mechanisms, Influencing Factors, and New Technique. *J. Hazard. Mater.* **2021**, *418*, 126313. https://doi.org/10.1016/j.jhazmat.2021.126313.

(10) Jasmann, J. R.; Borch, T.; Sale, T. C.; Blotevogel, J. Advanced Electrochemical Oxidation of 1,4-Dioxane via Dark Catalysis by Novel Titanium Dioxide (TiO_2) Pellets. *Environ. Sci. Technol.* **2016**, *50* (16), 8817–8826. https://doi.org/10.1021/acs.est.6b02183.

(11) De Clercq, J.; Van de Steene, E.; Verbeken, K.; Verhaege, M. Electrochemical Oxidation of 1,4-Dioxane at Boron-Doped Diamond Electrode. *J. Chem. Technol. Biotechnol.* **2010**, *85* (8), 1162–1167. https://doi.org/10.1002/jctb.2415.

(12) Mameda, N.; Park, H.; Shah, S. S. A.; Lee, K.; Li, C.-W.; Naddeo, V.; Choo, K.-H. Highly Robust and Efficient Ti-Based Sb-SnO_2 Anode with a Mixed Carbon and Nitrogen Interlayer for Electrochemical 1,4-Dioxane Removal from Water. *Chem. Eng. J.* **2020**, *393*, 124794. https://doi.org/10.1016/j.cej.2020.124794.

(13) Park, H.; Mameda, N.; Choo, K.-H. Catalytic Metal Oxide Nanopowder Composite Ti Mesh for Electrochemical Oxidation of 1,4-Dioxane and Dyes. *Chem. Eng. J.* **2018**, *345*, 233–241. https://doi.org/10.1016/j.cej.2018.03.158.

(14) Li, W.; Xiao, R.; Xu, J.; Lin, H.; Yang, K.; Li, W.; He, K.; Tang, L.; Chen, J.; Wu, Y.; Lv, S. Interface Engineering Strategy of a Ti_4O_7 Ceramic Membrane via Graphene Oxide

Nanoparticles toward Efficient Electrooxidation of 1,4-Dioxane. *Water Res.* **2022**, *216*, 118287. https://doi.org/10.1016/j.watres.2022.118287.
(15) Barndõk, H.; Hermosilla, D.; Negro, C.; Blanco, Á. Comparison and Predesign Cost Assessment of Different Advanced Oxidation Processes for the Treatment of 1,4-Dioxane-Containing Wastewater from the Chemical Industry. *ACS Sustain. Chem. Eng.* **2018**, *6* (5), 5888–5894. https://doi.org/10.1021/acssuschemeng.7b04234.
(16) Sirés, I.; Brillas, E. Electro-Fenton Process: Fundamentals and Reactivity. In *Electro-Fenton Process: New Trends and Scale-Up*; Zhou, M., Oturan, M. A., Sirés, I., Eds.; The Handbook of Environmental Chemistry; Springer: Singapore, 2018; pp 1–28. https://doi.org/10.1007/698_2017_40.
(17) Xue, S.; Sun, S.; Qing, W.; Huang, T.; Liu, W.; Liu, C.; Yao, H.; Zhang, W. Experimental and Computational Assessment of 1,4-Dioxane Degradation in a Photo-Fenton Reactive Ceramic Membrane Filtration Process. *Front. Environ. Sci. Eng.* **2021**, *15* (5), 95. https://doi.org/10.1007/s11783-020-1341-y.
(18) Plakas, K. V.; Karabelas, A. J. Electro-Fenton Applications in the Water Industry. In *Electro-Fenton Process*; Zhou, M., Oturan, M. A., Sirés, I., Eds.; The Handbook of Environmental Chemistry; Springer Singapore: Singapore, 2017; Vol. 61, pp 343–378. https://doi.org/10.1007/698_2017_52.
(19) Sheng, H.; Janes, A.; Ross, R.; Hofstetter, H.; Lee, K.; Schmidt, J.; Jin, S. Linear Paired Electrochemical Valorization of Glycerol Enabled by the Electro-Fenton Process Using a Stable $NiSe_2$ Cathode. *Nat. Catal.* **2022**, *5*, 716–725. https://doi.org/10.1038/s41929-022-00826-y.
(20) Perry, S. C.; Pangotra, D.; Vieira, L.; Csepei, L.-I.; Sieber, V.; Wang, L.; Ponce de León, C.; Walsh, F. C. Electrochemical Synthesis of Hydrogen Peroxide from Water and Oxygen. *Nat. Rev. Chem.* **2019**, *3* (7), 442–458. https://doi.org/10.1038/s41570-019-0110-6.
(21) Yang, X.; Zeng, Y.; Alnoush, W.; Hou, Y.; Higgins, D.; Wu, G. Tuning Two-Electron Oxygen-Reduction Pathways for H2O2 Electrosynthesis via Engineering Atomically Dispersed Single Metal Site Catalysts. *Adv. Mater.* **2022**, *34* (23), 2107954. https://doi.org/10.1002/adma.202107954.
(22) Zhang, D.; Mitchell, E.; Lu, X.; Chu, D.; Shang, L.; Zhang, T.; Amal, R.; Han, Z. Metal-Free Carbon-Based Catalysts Design for Oxygen Reduction Reaction towards Hydrogen Peroxide: From 3D to 0D. *Mater. Today* **2023**, *63*, 339–359. https://doi.org/10.1016/j.mattod.2023.02.004.
(23) Shen, R.; Chen, W.; Peng, Q.; Lu, S.; Zheng, L.; Cao, X.; Wang, Y.; Zhu, W.; Zhang, J.; Zhuang, Z.; Chen, C.; Wang, D.; Li, Y. High-Concentration Single Atomic Pt Sites on Hollow CuSx for Selective O_2 Reduction to H_2O_2 in Acid Solution. *Chem* **2019**, *5* (8), 2099–2110. https://doi.org/10.1016/j.chempr.2019.04.024.
(24) Kim, H.-E.; Lee, I. H.; Cho, J.; Shin, S.; Ham, H. C.; Kim, J. Y.; Lee, H. Palladium Single-Atom Catalysts Supported on $C@C_3N_4$ for Electrochemical Reactions. *ChemElectroChem* **2019**, *6* (18), 4757–4764. https://doi.org/10.1002/celc.201900772.
(25) Ledendecker, M.; Pizzutilo, E.; Malta, G.; Fortunato, G. V.; Mayrhofer, K. J. J.; Hutchings, G. J.; Freakley, S. J. Isolated Pd Sites as Selective Catalysts for Electrochemical and Direct Hydrogen Peroxide Synthesis. *ACS Catal.* **2020**, *10* (10), 5928–5938. https://doi.org/10.1021/acscatal.0c01305.
(26) Sun, Y.; Sinev, I.; Ju, W.; Bergmann, A.; Dresp, S.; Kühl, S.; Spöri, C.; Schmies, H.; Wang, H.; Bernsmeier, D.; Paul, B.; Schmack, R.; Kraehnert, R.; Roldan Cuenya, B.; Strasser, P. Efficient Electrochemical Hydrogen Peroxide Production from Molecular Oxygen on Nitrogen-Doped

Mesoporous Carbon Catalysts. *ACS Catal.* **2018**, *8* (4), 2844–2856. https://doi.org/10.1021/acscatal.7b03464.
(27) Jung, E.; Shin, H.; Lee, B.-H.; Efremov, V.; Lee, S.; Lee, H. S.; Kim, J.; Hooch Antink, W.; Park, S.; Lee, K.-S.; Cho, S.-P.; Yoo, J. S.; Sung, Y.-E.; Hyeon, T. Atomic-Level Tuning of Co–N–C Catalyst for High-Performance Electrochemical H2O2 Production. *Nat. Mater.* **2020**, *19* (4), 436–442. https://doi.org/10.1038/s41563-019-0571-5.
(28) Zhao, K.; Su, Y.; Quan, X.; Liu, Y.; Chen, S.; Yu, H. Enhanced H2O2 Production by Selective Electrochemical Reduction of O_2 on Fluorine-Doped Hierarchically Porous Carbon. *J. Catal.* **2018**, *357*, 118–126. https://doi.org/10.1016/j.jcat.2017.11.008.
(29) Sheng, Y.; Song, S.; Wang, X.; Song, L.; Wang, C.; Sun, H.; Niu, X. Electrogeneration of Hydrogen Peroxide on a Novel Highly Effective Acetylene Black-PTFE Cathode with PTFE Film. *Electrochimica Acta* **2011**, *56* (24), 8651–8656. https://doi.org/10.1016/j.electacta.2011.07.069.
(30) Sheng, H.; Hermes, E. D.; Yang, X.; Ying, D.; Janes, A. N.; Li, W.; Schmidt, J. R.; Jin, S. Electrocatalytic Production of H_2O_2 by Selective Oxygen Reduction Using Earth-Abundant Cobalt Pyrite (CoS2). *ACS Catal.* **2019**, *9* (9), 8433–8442. https://doi.org/10.1021/acscatal.9b02546.
(31) Lu, Z.; Chen, G.; Siahrostami, S.; Chen, Z.; Liu, K.; Xie, J.; Liao, L.; Wu, T.; Lin, D.; Liu, Y.; Jaramillo, T. F.; Nørskov, J. K.; Cui, Y. High-Efficiency Oxygen Reduction to Hydrogen Peroxide Catalysed by Oxidized Carbon Materials. *Nat. Catal.* **2018**, *1* (2), 156–162. https://doi.org/10.1038/s41929-017-0017-x.
(32) Adler, Z.; Zhang, X.; Feng, G.; Shi, Y.; Zhu, P.; Xia, Y.; Shan, X.; Wang, H. Hydrogen Peroxide Electrosynthesis in a Strong Acidic Environment Using Cationic Surfactants. *Precis. Chem.* **2024**. https://doi.org/10.1021/prechem.3c00096.
(33) Gyenge, E. L.; Oloman, C. W. Influence of Surfactants on the Electroreduction of Oxygen to Hydrogen Peroxide in Acid and Alkaline Electrolytes. *J. Appl. Electrochem.* **2001**, *31* (2), 233–243. https://doi.org/10.1023/A:1004159102510.
(34) Zhang, X.; Zhao, X.; Zhu, P.; Adler, Z.; Wu, Z.-Y.; Liu, Y.; Wang, H. Electrochemical Oxygen Reduction to Hydrogen Peroxide at Practical Rates in Strong Acidic Media. *Nat. Commun.* **2022**, *13* (1), 2880. https://doi.org/10.1038/s41467-022-30337-0.
(35) García de Arquer, F. P.; Dinh, C.-T.; Ozden, A.; Wicks, J.; McCallum, C.; Kirmani, A. R.; Nam, D.-H.; Gabardo, C.; Seifitokaldani, A.; Wang, X.; Li, Y. C.; Li, F.; Edwards, J.; Richter, L. J.; Thorpe, S. J.; Sinton, D.; Sargent, E. H. CO_2 Electrolysis to Multicarbon Products at Activities Greater than 1 A Cm^{-2}. *Science* **2020**, *367* (6478), 661–666. https://doi.org/10.1126/science.aay4217.
(36) Ding, P.; An, H.; Zellner, P.; Guan, T.; Gao, J.; Müller-Buschbaum, P.; Weckhuysen, B. M.; van der Stam, W.; Sharp, I. D. Elucidating the Roles of Nafion/Solvent Formulations in Copper-Catalyzed CO_2 Electrolysis. *ACS Catal.* **2023**, *13* (8), 5336–5347. https://doi.org/10.1021/acscatal.2c05235.
(37) Nidheesh, P. V.; Zhou, M.; Oturan, M. A. An Overview on the Removal of Synthetic Dyes from Water by Electrochemical Advanced Oxidation Processes. *Chemosphere* **2018**, *197*, 210–227. https://doi.org/10.1016/j.chemosphere.2017.12.195.
(38) Scialdone, O. Electrochemical Oxidation of Organic Pollutants in Water at Metal Oxide Electrodes: A Simple Theoretical Model Including Direct and Indirect Oxidation Processes at the Anodic Surface. *Electrochimica Acta* **2009**, *54* (26), 6140–6147. https://doi.org/10.1016/j.electacta.2009.05.066.

(39) Comninellis, C. Electrocatalysis in the Electrochemical Conversion/Combustion of Organic Pollutants for Waste Water Treatment. *Electrochimica Acta* **1994**, *39* (11–12), 1857–1862. https://doi.org/10.1016/0013-4686(94)85175-1.
(40) Martínez-Huitle, C. A.; Andrade, L. S. Electrocatalysis in Wastewater Treatment: Recent Mechanism Advances. *Quím. Nova* **2011**, *34* (5), 850–858. https://doi.org/10.1590/S0100-40422011000500021.
(41) Mavrikis, S.; Perry, S. C.; Leung, P. K.; Wang, L.; Ponce de León, C. Recent Advances in Electrochemical Water Oxidation to Produce Hydrogen Peroxide: A Mechanistic Perspective. *ACS Sustain. Chem. Eng.* **2021**, *9* (1), 76–91. https://doi.org/10.1021/acssuschemeng.0c07263.
(42) Kim, C.; Park, S. O.; Kwak, S. K.; Xia, Z.; Kim, G.; Dai, L. Concurrent Oxygen Reduction and Water Oxidation at High Ionic Strength for Scalable Electrosynthesis of Hydrogen Peroxide. *Nat. Commun.* **2023**, *14* (1), 5822. https://doi.org/10.1038/s41467-023-41397-1.
(43) Kelly, S. R.; Shi, X.; Back, S.; Vallez, L.; Park, S. Y.; Siahrostami, S.; Zheng, X.; Nørskov, J. K. ZnO As an Active and Selective Catalyst for Electrochemical Water Oxidation to Hydrogen Peroxide. *ACS Catal.* **2019**, *9* (5), 4593–4599. https://doi.org/10.1021/acscatal.8b04873.
(44) Yoshida, T.; Komatsu, D.; Shimokawa, N.; Minoura, H. Mechanism of Cathodic Electrodeposition of Zinc Oxide Thin Films from Aqueous Zinc Nitrate Baths. *Thin Solid Films* **2004**, *451–452*, 166–169. https://doi.org/10.1016/j.tsf.2003.10.097.
(45) Pashkova, A.; Svajda, K.; Black, G.; Dittmeyer, R. Automated System for Spectrophotometric Detection of Liquid Phase Hydrogen Peroxide for Concentrations up to 5% w/w. *Rev. Sci. Instrum.* **2009**, *80* (5), 055104. https://doi.org/10.1063/1.3120523.
(46) Vafaei Molamahmood, H.; Geng, W.; Wei, Y.; Miao, J.; Yu, S.; Shahi, A.; Chen, C.; Long, M. Catalyzed H_2O_2 Decomposition over Iron Oxides and Oxyhydroxides: Insights from Oxygen Production and Organic Degradation. *Chemosphere* **2022**, *291*, 133037. https://doi.org/10.1016/j.chemosphere.2021.133037.
(47) Brillas, E.; Sirés, I.; Oturan, M. A. Electro-Fenton Process and Related Electrochemical Technologies Based on Fenton's Reaction Chemistry. *Chem. Rev.* **2009**, *109* (12), 6570–6631. https://doi.org/10.1021/cr900136g.
(48) Fan, L.; Bai, X.; Xia, C.; Zhang, X.; Zhao, X.; Xia, Y.; Wu, Z.-Y.; Lu, Y.; Liu, Y.; Wang, H. CO_2/Carbonate-Mediated Electrochemical Water Oxidation to Hydrogen Peroxide. *Nat. Commun.* **2022**, *13* (1), 2668. https://doi.org/10.1038/s41467-022-30251-5.
(49) Shafirovich, V.; Dourandin, A.; Huang, W.; Geacintov, N. E. The Carbonate Radical Is a Site-Selective Oxidizing Agent of Guanine in Double-Stranded Oligonucleotides. *J. Biol. Chem.* **2001**, *276* (27), 24621–24626. https://doi.org/10.1074/jbc.M101131200.
(50) Pica, N. E.; Miao, Y.; Johnson, N. W.; Ramos, P.; Mahendra, S.; Blotevogel, J. Bioelectrochemical Treatment of 1,4-Dioxane in the Presence of Chlorinated Solvents: Design, Process, and Sustainability Considerations. *ACS Sustain. Chem. Eng.* **2021**, *9* (8), 3172–3182. https://doi.org/10.1021/acssuschemeng.0c08152.
(51) Yuan, J.; Yin, H.; Ge, X.; Pan, R.; Huang, C.; Chen, D.; Hu, L.; Xie, H. Superior Efficiency Hydrogen Peroxide Production in Acidic Media through Epoxy Group Adjacent to Co-O/C Active Centers on Carbon Black. *Chem. Eng. J.* **2023**, *465*, 142691. https://doi.org/10.1016/j.cej.2023.142691.
(52) Pang, Y.; Wang, K.; Xie, H.; Sun, Y.; Titirici, M.-M.; Chai, G.-L. Mesoporous Carbon Hollow Spheres as Efficient Electrocatalysts for Oxygen Reduction to Hydrogen Peroxide in Neutral Electrolytes. *ACS Catal.* **2020**, *10* (14), 7434–7442. https://doi.org/10.1021/acscatal.0c00584.

(53) Tong, Y.; Liu, J.; Su, B.-J.; Juang, J.-Y.; Hou, F.; Yin, L.; Dou, S. X.; Liang, J. High-Rate Electrochemical H_2O_2 Production over Multimetallic Atom Catalysts under Acidic–Neutral Conditions. *Carbon Energy* **2024**, *6* (1), e378. https://doi.org/10.1002/cey2.378.
(54) Iglesias, D.; Giuliani, A.; Melchionna, M.; Marchesan, S.; Criado, A.; Nasi, L.; Bevilacqua, M.; Tavagnacco, C.; Vizza, F.; Prato, M.; Fornasiero, P. N-Doped Graphitized Carbon Nanohorns as a Forefront Electrocatalyst in Highly Selective O_2 Reduction to H_2O_2. *Chem* **2018**, *4* (1), 106–123. https://doi.org/10.1016/j.chempr.2017.10.013.
(55) Zhang, C.; Shen, W.; Guo, K.; Xiong, M.; Zhang, J.; Lu, X. A Pentagonal Defect-Rich Metal-Free Carbon Electrocatalyst for Boosting Acidic O2 Reduction to H_2O_2 Production. *J. Am. Chem. Soc.* **2023**, *145* (21), 11589–11598. https://doi.org/10.1021/jacs.3c00689.
(56) Liang, J.; Wang, Y.; Liu, Q.; Luo, Y.; Li, T.; Zhao, H.; Lu, S.; Zhang, F.; Asiri, A. M.; Liu, F.; Ma, D.; Sun, X. Electrocatalytic Hydrogen Peroxide Production in Acidic Media Enabled by NiS_2 Nanosheets. *J. Mater. Chem. A* **2021**, *9* (10), 6117–6122. https://doi.org/10.1039/D0TA12008A.
(57) Kim, J. H.; Shin, D.; Lee, J.; Baek, D. S.; Shin, T. J.; Kim, Y.-T.; Jeong, H. Y.; Kwak, J. H.; Kim, H.; Joo, S. H. A General Strategy to Atomically Dispersed Precious Metal Catalysts for Unravelling Their Catalytic Trends for Oxygen Reduction Reaction. *ACS Nano* **2020**, *14* (2), 1990–2001. https://doi.org/10.1021/acsnano.9b08494.
(58) Zhao, X.; Yin, Q.; Mao, X.; Cheng, C.; Zhang, L.; Wang, L.; Liu, T.-F.; Li, Y.; Li, Y. Theory-Guided Design of Hydrogen-Bonded Cobaltoporphyrin Frameworks for Highly Selective Electrochemical H_2O_2 Production in Acid. *Nat. Commun.* **2022**, *13* (1), 2721. https://doi.org/10.1038/s41467-022-30523-0.
(59) Han, C.-D.; Zhang, Y.-C.; Zhang, Q.; Wu, J.-T.; Gao, J.; Zou, J.-J.; Zhu, X.-D. $NaBH_4$-Induced Phase Transition of $CoSe_2$ with Abundant Se Deficiency for Acidic Oxygen Reduction to Hydrogen Peroxide. *Rare Met.* **2023**, *43*, 500–510. https://doi.org/10.1007/s12598-023-02467-x.

Appendix A

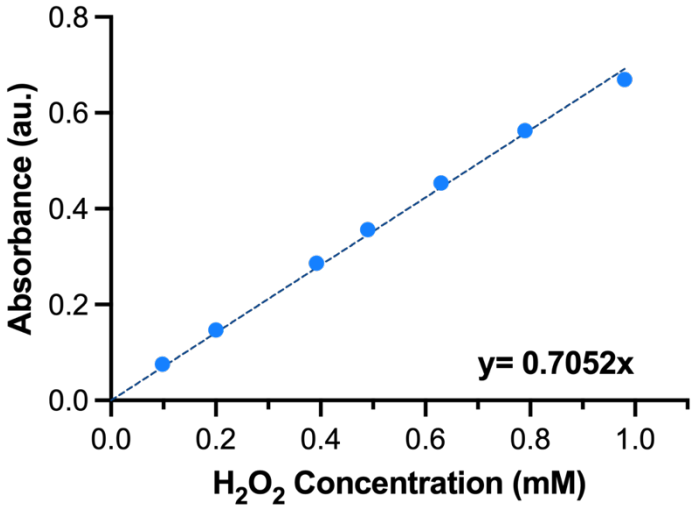


Figure 0-1- Calibration curve of H_2O_2/Ti complex. The wavelength of interest was 409nm. The R^2 value was 0.9915.

Table 3- Recently Developed Treatment Systems Utilizing AOPs for 1,4-Dioxane Degradation

Reactive Species	Reactive Species Generation	Reaction Conditions	Dioxane Oxidation	Reference
Conventional AOPSs				
Biodegradation (Electrochemically generated O_2)	Biodegradation by CB1190 and radical species (Ti/SnO_2-X)	Neutral with 100-500mg/L dioxane at 5.0V	99.9% by the end of the reactor	50

			No Product Analysis	
Oxidation by •OH	Photo-Fenton Process	Neutral with 2 mmol/L H_2O_2 at UV_{365} irradiation with 10.8 mg/L Dioxane	90% within 12 hours in batch reactor **No Product Analysis**	17
Oxidation by •OH	UV/H_2O_2	0.106 mg/L Dioxane with 10mg/L H_2O_2	~100% Dioxane Removal by 8 min **Quantitative Product Analysis**	8
Oxidation by and $\cdot O_2^-$	Photo-Fenton like using TiO_2 nanoparticles	Neutral with 10mg/L Dioxane at 6.58mW/cm^2 light intensity	99.99% Dioxane Degradation by 4hr **No Product Analysis**	4
Electrochemical Processes				

Reactive Species	**Electrodes**	**Electrochemical conditions**	**Dioxane Oxidation**	**Product Analysis Done**
Suggested oxidation by •OH	Ti/TiONC/Sb-SnO_2	0.1 M Na_2SO_4 with 10mg/L 1,4-dioxane (Potential is at least 2.06V)	~100% Dioxane Degradation by 120 min **No Product Analysis**	12
Oxidation by •OH	BDD	0.1M Na_2SO_4 at 6V with 0.1M dioxane	~100% Dioxane Removal by 2 hr **No Product Analysis**	13
Oxidation by •OH	1%GONs@Ti_4O_7	0.02 M Na_2SO_4 at 6V with 0.01M dioxane	63.2% Dioxane Removal in 0.012 h **No Product Analysis**	14
Oxidation by •OH	TiO_2	0.03M Na_2SO_4 at 8V with 0.34mM Dioxane	85.2% Dioxane Removal in Single Pass	10

			Qualitative Product Analysis (Product Identification)	

Table 4- List of Electrocatalysts Recently Developed for 2e- ORR in Acidic Media with the Electrolyte Used in the System, Onset Potential, FE% at Greatest Current Density, and the Percentage of Nafion (w/w%) Used in the Catalyst Ink

Electrocatalyst	Electrolyte	pH	Onset (RHE)	Current Density (mA/cm^2)	Potential (V vs RHE)	FE%	Nafion (%)	Reference
Non-Metal								
N-doped C	0.5M H_2SO_4	0.3	0.4	-1.4	0.1	93		26
F-doped C	0.05M H_2SO_4	1.3	0.2	-2.5	-0.3	89	28	28
O-doped carbon nanotubes	0.1M $HClO_4$	1.0	0.2	-0.45	0.1	53	-	31

Carbon Black	0.05M H_2SO_4	1.3	0.2	-0.2	0	88	37	51
Mesoporous Carbon Hollow Spheres	0.5M H_2SO_4	0.3	0.3	-2.25	0	70	-	52
N-doped Carbon	0.1M $HClO_4$	1.5	0.5	-0.8	0	69	31	53
N-doped Carbon	0.1M H_2SO_4	1.0	0.4	-0.3	0.3	97	840	54
Pentagon-rich N-doped carbon	0.1M $HClO_4$	1.0	0.5	-3	0.1	98	-	55
Metal-Based Catalysts								
h-Pt/CuS_x	0.1M $HClO_4$	1.0	0.6	-2.9	0.1	92	23	23
CoS_2	0.05M H_2SO_4	1.3	0.69	-4.2	0	18	517	30
Co/N-doped Graphene	0.1M $HClO_4$	1.0	0.7	-3.75	0.2	50	230	27

NiS_2	0.05M H_2SO_4	1.3	0.5	-8	0.15	69	28	[56]
$PdCl_x/C$	0.1M $HClO_4$	1.0	0.6	-1.4	0.2	90	-	[25]
0.5% PdC/C_3N_4	0.1M $HClO_4$	1.0	0.5	-3	0.2	85	18	[24]
Pt/Carbon nanotubes	0.1M $HClO_4$	1.0	0.4	-2	0.2	60	39	[57]
Co/O-doped Carbon Black	0.05M H_2SO_4	1.3	0.5	-2.7	0	65	37	[51]
Ni-/O-doped Carbon Black	0.05M H_2SO_4	1.3	0.3	-1.4	0	70	37	[51]
Co_x-Ni	0.1M $HClO_4$	1.5	0.5	-2.1	0	79	31	[53]
Cobaltoporphyrin	0.1M $HClO_4$	1.5	0.5	-3	0.1	95	18	[58]
c-$CoSe_2$	0.1M $HClO_4$	1.0	0.6	-3	0	85	-	[59]

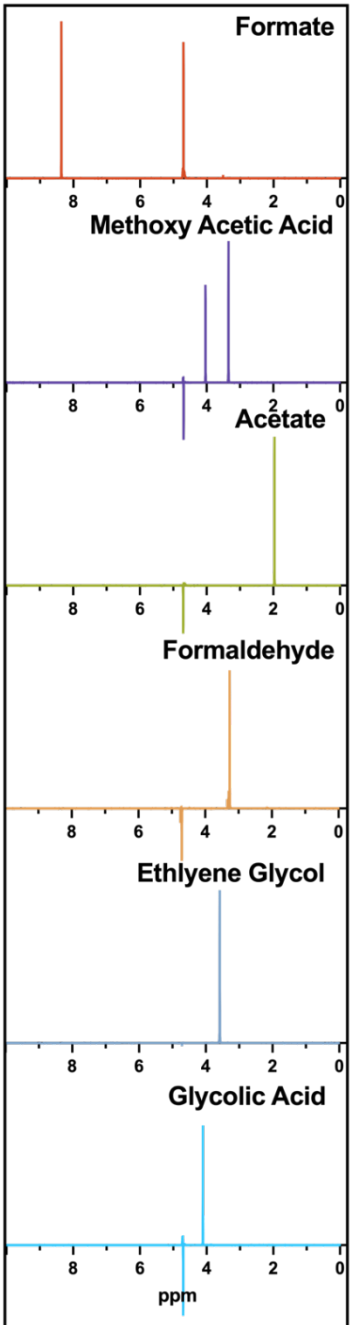


Figure 0-2- NMR Standards of Common Dioxane Oxidation Products as Determined by Jasmeen et al

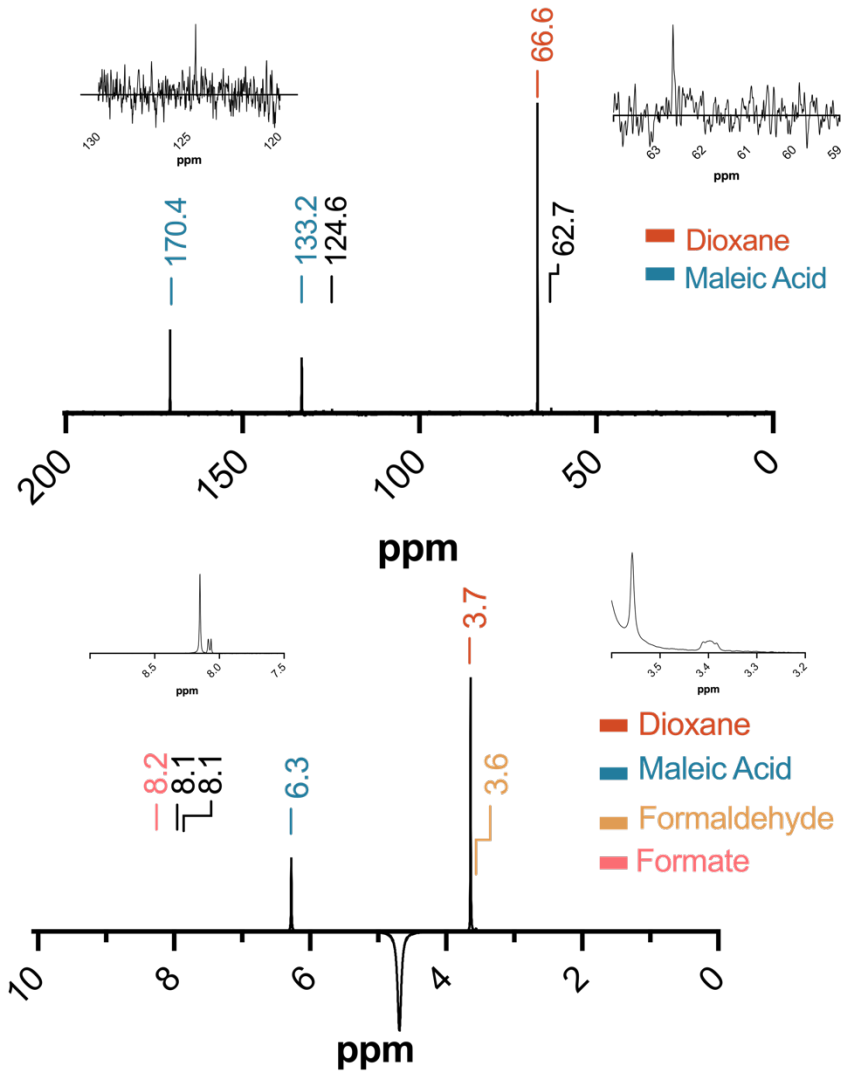


Figure 0-3- ^{13}C NMR (top) and ^{1}H NMR (bottom) of EF reaction at 3mM Fe^{2+} after 500C has passed. Peaks of interest are identified.

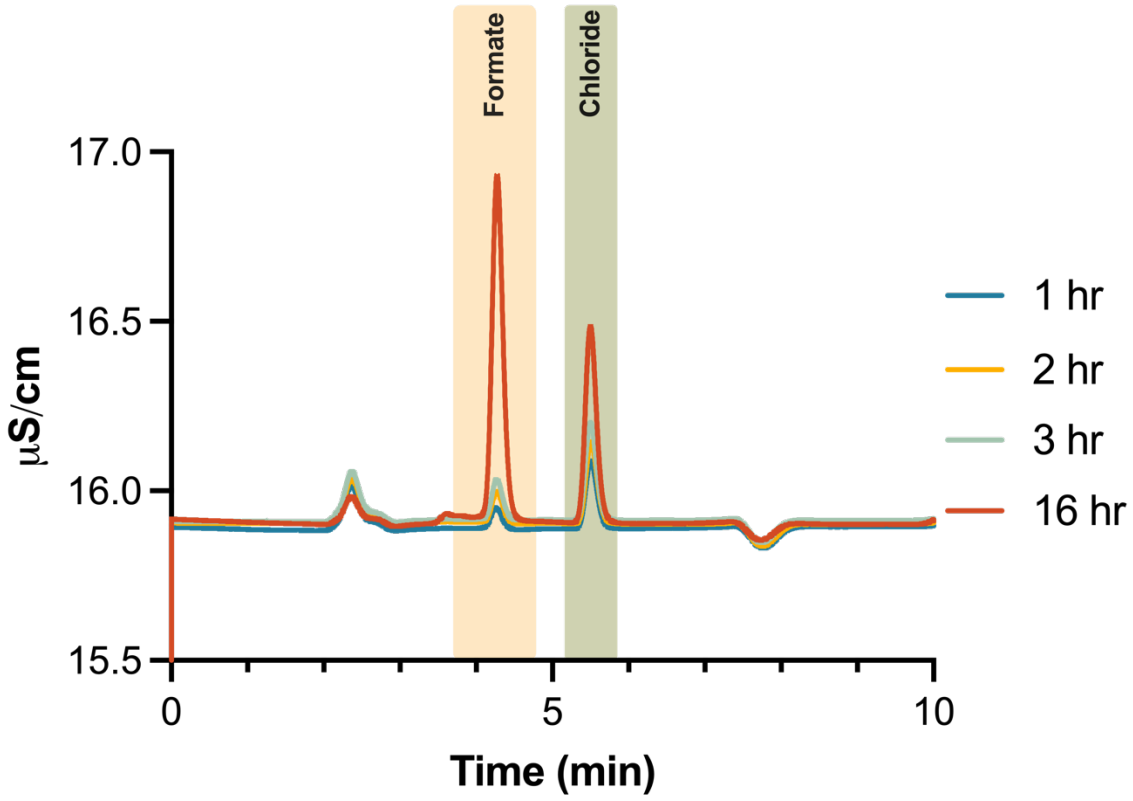


Figure 0-4- IC results containing ionic products formed during long-term EF reaction at 5mM Fe^{2+}